1975

Petrography of Precambrian iron formation, Pembina County, North Dakota

Ronald E. Richardson
University of North Dakota

PETROGRAPHY OF PRECAMBRIAN IRON FORMATION, PEMBINA COUNTY, NORTH DAKOTA

by

Ronald E. Richardson

Bachelor of Science, University of Wisconsin, 1968

A Thesis

Submitted to the Graduate Faculty

of the

University of North Dakota

in partial fulfillment of the requirements

for the degree of

Master of Science

Grand Forks, North Dakota

May
1975

PETROGRAPHY OF PRECAMBRIAN IRON FORMATION,
PEMBINA COUNTY, NORTH DAKOTA

Ronald E. Richardson, Master of Science

The University of North Dakota, 1975

Faculty Advisor: Professor Frank Karner

In October of 1964 the Topographic Branch of the United States Geological Survey reported difficulties in using magnetic compasses while mapping in the areas of Akra and Hensel, Pembina County, North Dakota. University of North Dakota geologists located anomalies of 67,500 gammas 1.6 km east of Akra and 71,500 gammas 4 km east of Hensel, the normal magnetic field in this area being about 60,000 gammas. The rock bodies producing the magnetic anomalies were drilled and examination of diamond drill core showed them to consist of oxide and silicate facies iron formation interlayered with quartz-biotite schist of Precambrian age. The core recovered from the Akra site contained mineral assemblages of the greenschist and amphibolite facies of regional metamorphism, the metamorphic grade increasing with depth. The mineral assemblages of the Hensel core indicate amphibolite facies metamorphism. The Precambrian rocks of eastern North Dakota represent the subsurface extension of the Superior Province of the Canadian Shield. This province is characterized by linear greenstone belts of metavolcanics and metasediments separated by areas of intrusive, felsic igneous rocks. Similarities between the Akra and Hensel rock bodies and iron formations exposed on the Canadian Shield suggest deposition during the sedimentary phase of greenstone belt evolution.

This thesis submitted by Ronald E. Richardson in partial fulfillment of the requirements for the Degree of Master of Science from the University of North Dakota is hereby approved by the Faculty Advisory Committee under whom the work has been done.

(Chairman)

Dean of the Graduate School

Permission

Title PETROGRAPHY OF PRECAMBRIAN IRON FORMATION, PEMBINA COUNTY, NORTH DAKOTA

Department Geology

Degree Master of Science

In presenting this thesis in partial fulfillment of the requirements for a graduate degree from the University of North Dakota, I agree that the Library of this University shall make it freely available for inspection. I further agree that permission for extensive copying for scholarly purposes may be granted by the professor who supervised my thesis work or, in his absence, by the Chairman of the Department or the Dean of the Graduate School. It is understood that any copying or publication or other use of this thesis or part thereof for financial gain shall not be allowed without my written permission. It is also understood that due recognition shall be given to me and to the University of North Dakota in any scholarly use which may be made of any material in my thesis.

Signature _____

Date _____

ACKNOWLEDGMENTS

I would like to thank Professors Frank Karner, Walter L. Moore, and N. N. Kohanowski for serving on my committee and my thanks to the Geology Department of the University of North Dakota for its facilities and its grant of a graduate teaching assistantship to the author.

TABLE OF CONTENTS

LIST OF TABLES

LIST OF ILLUSTRATIONS

ABSTRACT

In October of 1964 the Topographic Branch of the United States Geological Survey reported difficulties in using magnetic compasses while mapping in the areas of Akra and Hensel, Pembina County, North Dakota. University of North Dakota geologists located anomalies of 67,500 gammas 1.6 km east of Akra and 71,500 gammas 4 km east of Hensel, the normal magnetic field in this area being about 60,000 gammas. The rock bodies producing the magnetic anomalies were drilled and examination of diamond drill core showed them to consist of oxide and silicate facies iron formation interlayered with quartz-biotite schist of Precambrian age. The core recovered from the Akra site contained mineral assemblages of the greenschist and amphibolite facies of regional metamorphism, the metamorphic grade increasing with depth. The mineral assemblages of the Hensel core indicate amphibolite facies metamorphism. The Precambrian rocks of eastern North Dakota represent the subsurface extension of the Superior Province of the Canadian Shield. This province is characterized by linear greenstone belts of metavolcanics and metasediments separated by areas of intrusive, felsic igneous rocks. Similarities between the Akra and Hensel rock bodies and iron formations exposed on the Canadian Shield suggest deposition during the sedimentary phase of greenstone belt evolution.

INTRODUCTION

In October of 1964 the Topographic Branch of the United States Geological Survey reported difficulties in using magnetic compasses while mapping in the areas of Akra and Hensel in Pembina County, North Dakota (Moore and Karner, 1969). In the late fall of 1964, University of North Dakota geologists located anomalies of 67,500 gammas 1.6 km east of Akra and 71,500 gammas 4 km east of Hensel, the normal magnetic field in this area being about 60,000 gammas. In the summer of 1966 the anomalies were mapped in detail (Figure 1).

Moore and Karner (1969) speculated that the anomalies were due to the presence of hematite bodies, magnetite disseminated in gabbros or similar rocks, or magnetite-rich rocks of igneous or replacement origin. They concluded, on the basis of areal extent and magnetic field gradients, that the anomalies were probably due to the latter.

In July of 1966, prompted by the possibility of discovering economic ore deposits, the rock bodies producing the magnetic anomalies were drilled by the Amerada-Hess Petroleum Corporation. At the Akra drilling site, Amerada #1 Sig Samson test in SE¼ Sec. 11, T.161N., R.55W., a 106.1 m interval of the Precambrian basement was cored. At the Hensel drilling site, Amerada #1 H. Sellheim test in NE¼ Sec. 8, T.160N., R.54W., a 212.1 m interval of the Precambrian basement was cored. Examination of NX diamond drill core from the two sites showed that the magnetic anomalies were caused by iron-rich metasedimentary rocks of Precambrian age.

Fig. 1. Location Map and Map of the Akra and Hensel Magnetic Anomalies, Pembina County, North Dakota (after Moore and Karner, 1969).

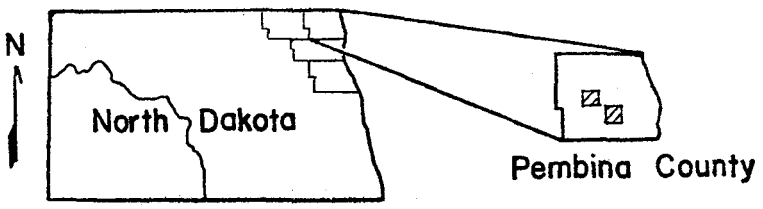

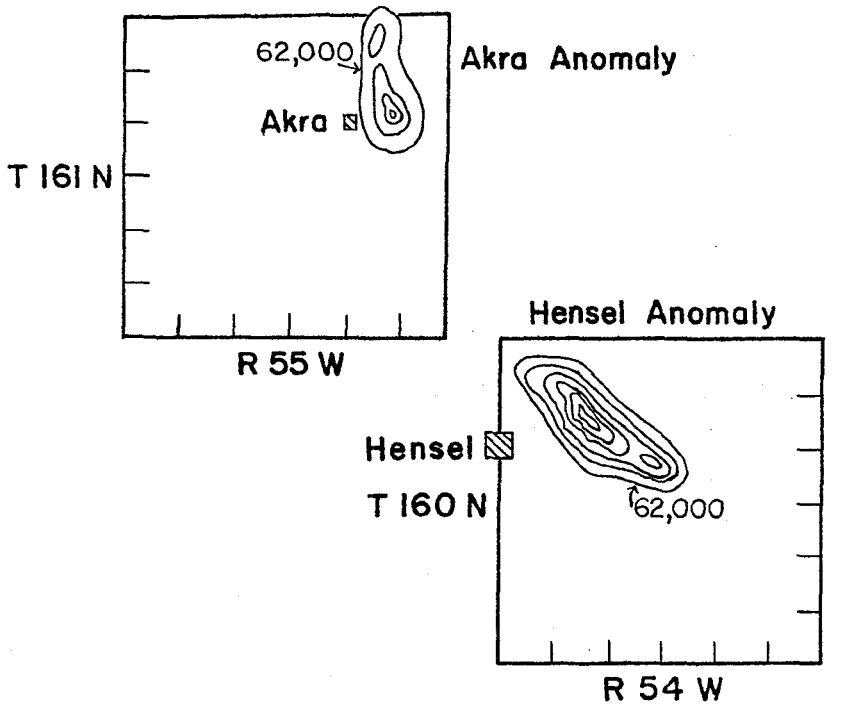

Contour Interval = 2000 gammas (Total Field)

Vertical variations in mineralogy were studied and lithologic units recognized. Types of iron formation were recognized on the basis of the iron minerals present. The mineralogy of the iron-bearing units was used to place each into a geochemical facies indicative of environment of deposition as defined by James (1966). Metastable mineral assemblages were defined and two facies of regional metamorphism were recognized. Metamorphic reactions leading to the observed end-products were postulated. These, coupled with textural evidence, have led to a hypothesis on the conditions of deposition and metamorphism of these rock bodies.

REGIONAL PRECAMBRIAN GEOLOGY

North Dakota is located between exposed Precambrian rocks in Minnesota, South Dakota, Montana, Wyoming, and the Canadian Shield. There are no exposed Precambrian rocks in the state. The character of the Precambrian of North Dakota is known only from approximately 110 wells which have penetrated the basement complex. The majority of these wells are located in the eastern half of the state, the Precambrian of western North Dakota being overlain by the thick sedimentary sequence of the Williston basin. At the Minnesota border, the Precambrian surface is generally buried to a depth of about 300 m or less and dips westward at about 7 m to 9 m per km to a maximum depth of about 5090 m in the Williston basin (Lidiak, in preparation).

The Precambrian of North Dakota represents the subsurface extensions of two provinces of the Canadian Shield (Lidiak, in preparation). Eastern North Dakota is underlain by rocks of the Superior Province and western North Dakota by rocks of the younger Churchill Province. The boundary between the two provinces runs north-south approximately through the center of the state (Lidiak, in preparation).

Precambrian rocks of Minnesota are characterized by northeast-southwest trending greenstone belts, composed of metavolcanic and metasedimentary rocks, which have been intruded by large volumes of igneous rocks of granitic to granodioritic composition (Sims, 1970). On the Bouger Gravity Anomaly Map of North Dakota (Woollard, 1964), these greenstone belts are gravity highs while the areas of felsic

igneous rocks are gravity lows. These gravity features can be traced into eastern North Dakota. Linear magnetic anomalies trending northeast-southwest are common and are caused by Precambrian iron formation associated with the greenstone belts (Schwartz and Prokopovitch, 1956). A detailed magnetic survey would probably show the extension of these trends into eastern North Dakota.

Utilizing available well samples and geophysical evidence, Lidiak (in preparation) has mapped the Precambrian rocks of the Superior Province which underlie eastern North Dakota. Because of insufficient data, no attempt was made to map western North Dakota.

Lidiak's map (in preparation) shows the Precambrian rocks of eastern North Dakota to conform to the general pattern seen in northern Minnesota. Northeast-southwest trending linear belts of metamorphic rocks, collectively referred to by Lidiak as amphibole schist terrane, are surrounded by large areas of intrusive igneous rocks which range in composition from granite to granodiorite. The rocks of the amphibole schist terrane are described as actinolite and hornblende schists and gneisses with subordinate serpentinite, all appearing to be of igneous origin and reflecting ultramafic, mafic, and intermediate igneous activity. Lidiak concludes that the amphibole schist terrane is similar to the greenstone belts of the Canadian Shield.

Three age dates from the Ramsey gneiss terrane of northeastern North Dakota and one from the McIntosh granite terrane of southeastern North Dakota yield ages from 2140 million years to 2570 million years (Lidiak, in preparation). These ages and the continuity of geophysical

trends discussed previously suggest that the Precambrian rocks of eastern North Dakota to be correlative with the Early Precambrian rocks of Northern Minnesota.

The basal (?) Early Precambrian Keewatin Group exposed in Northern Minnesota is composed of two formation: the Ely Greenstone and the Soudan Iron Formation (Van Hise and Clements, 1901). The Ely Greenstone consists of basaltic rocks (many showing pillow structures) and clastic material, possibly of pyroclastic origin. Its thickness is unknown (Goldich et al., 1961). The Soudan Iron Formation is composed of quartz, hematite, and martite or magnetite. Its thickness is unknown but is probably about 60 m (Klinger, 1956). Schwartz (1956) has suggested that the Soudan Iron Formation should be considered an iron-bearing member within and near the top of the Ely Greenstone, but Goldich et al. (1961) believe it deserves formational rank on the basis of its mappability. The Keewatin volcanics and sediments were intruded by felsic igneous rocks of the Laurentian orogeny 2400 to 2750 million years before the present, the largest intrusive body being the Saganaga Granite described by Grout (1929). The Keewatin rocks and Laurentian intrusives are unconformably overlain by the Knife Lake Group. This consists mainly of graywackes and slates, with arkoses, conglomerates, volcanic breccias, and minor iron formations (Goldich et al., 1961). The Knife Lake sediments were intruded by the Vermillion and Giant's Range Granites of the Algoman orogeny which occurred about 1600 to 1900 million years before the present.

METHODS

NX Diamond drill core from the two sites was studied in hand specimens and the core descriptions are included as Appendix A. Sixty-nine thin sections were studied petrographically. Modal analyses were made using a Leitz mechanical stage and 500 points per slide were counted (Appendices A and B). Reproducibility was determined by counting one slide five times (Table 1). Plagioclase determinations were made with the use of a five-axis universal stage following the methods of Moorhouse (1959) and Hutchison (1974).

Thirty-three samples were analyzed with a Philips X-ray diffractometer using copper k-alpha radiation. Diffraction patterns were run from two degrees to forty degrees two-theta. The X-ray results were used to verify optical identifications of minerals and to provide qualitative mineralogical information on intervals which were not thin-sectioned. The results are incorporated in Appendix A. Opaque minerals were studied in polished sections using polarized, reflected light. Etch tests were performed with HNO_3, HCL, KCN, $FeCl_3$, KOH, $HgCl_2$, and aqua regia using the methods described by Short (1940).

	VOLUME PERCENT					
	Quartz	Biotite	Clinozoisite	Pyrite	Plagioclase	Muscovite
Count 1	64.2	33.8	0.8	0.8	0.2	0.2
Count 2	68.4	29.2	1.2	0.6	0.4	0.2
Count 3	63.6	33.6	1.2	0.8	0.6	0.0
Count 4	66.0	31.2	1.6	0.4	0.4	0.4
Count 5	65.5	32.6	1.4	0.6	0.4	0.2
	M = 65.4	M = 32.1	M = 1.24	M = 0.64	M = 0.4	M = 0.2
	V = 2.79	V = 2.92	V = 0.07	V = 0.02	V = 0.02	V = 0.02
	SD = 1.67	SD = 1.71	SD = .27	SD = 0.15	SD = 0.13	SD = 0.13

PETROGRAPHY

Six rock types were recognized in the Akra and Hensel cores. Core descriptions including optical and X-ray data are given in Appendix A. Modal analyses are summarized in Appendix B. The stratigraphic distribution is summarized in Figures 2 and 3. The compositional and textural characteristics are given below.

Quartz-biotite Schist

Modal analyses of the quartz-biotite schist show this fine-grained rock contains 50-70 volume percent quartz, 10-30 percent biotite, usually less than 10 percent chlorite, 0-10 percent clinozoisite, 0-8 percent magnetite, less than 1 percent plagioclase, less than 1 percent almandite, and usually less than 1 percent pyrite (Figure 4).

Quartz, as grains 0.1-0.2 mm in diameter, is anhedral and usually equidimensional although some grains are slightly elongated parallel to schistosity. Quartz also occurs as porphyroblasts ranging up to 1 mm and giving the rock a seriate porphyroblastic texture. Subhedral biotite occurs as subparallel grains ranging from 0.03-0.3 mm in length. It is strongly pleochroic from light brown or light brownish-green through dark brown or dark brownish-green. Anhedral clinozoisite, 0.01-0.015 mm, occurs as disseminated grains and as veins. Subhedral plagioclase grains, 0.7-1 mm are present and exhibit albite twinning. Pericline and Carlsbad twinning are

Fig. 2. Stratigraphic Column of the Akra Core. Ground level elevation is 284 m above sea level. Depths are given in metres below ground level.

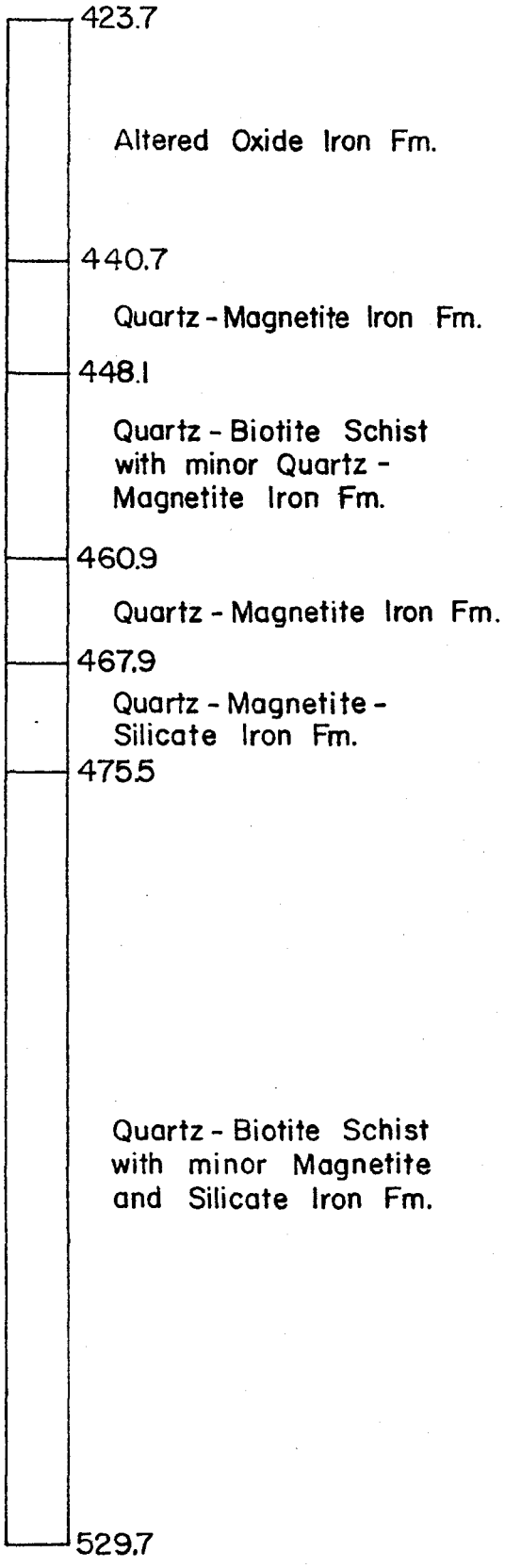
423.7
Altered Oxide Iron Fm.
440.7
Quartz - Magnetite Iron Fm.
448.1
Quartz - Biotite Schist with minor Quartz - Magnetite Iron Fm.
460.9
Quartz - Magnetite Iron Fm.
467.9
Quartz - Magnetite - Silicate Iron Fm.
475.5
Quartz - Biotite Schist with minor Magnetite and Silicate Iron Fm.
529.7

Fig. 3. Stratigraphic Column of the Hensel Core. Ground level elevation is 274 m above sea level. Depths are given in metres below ground level.

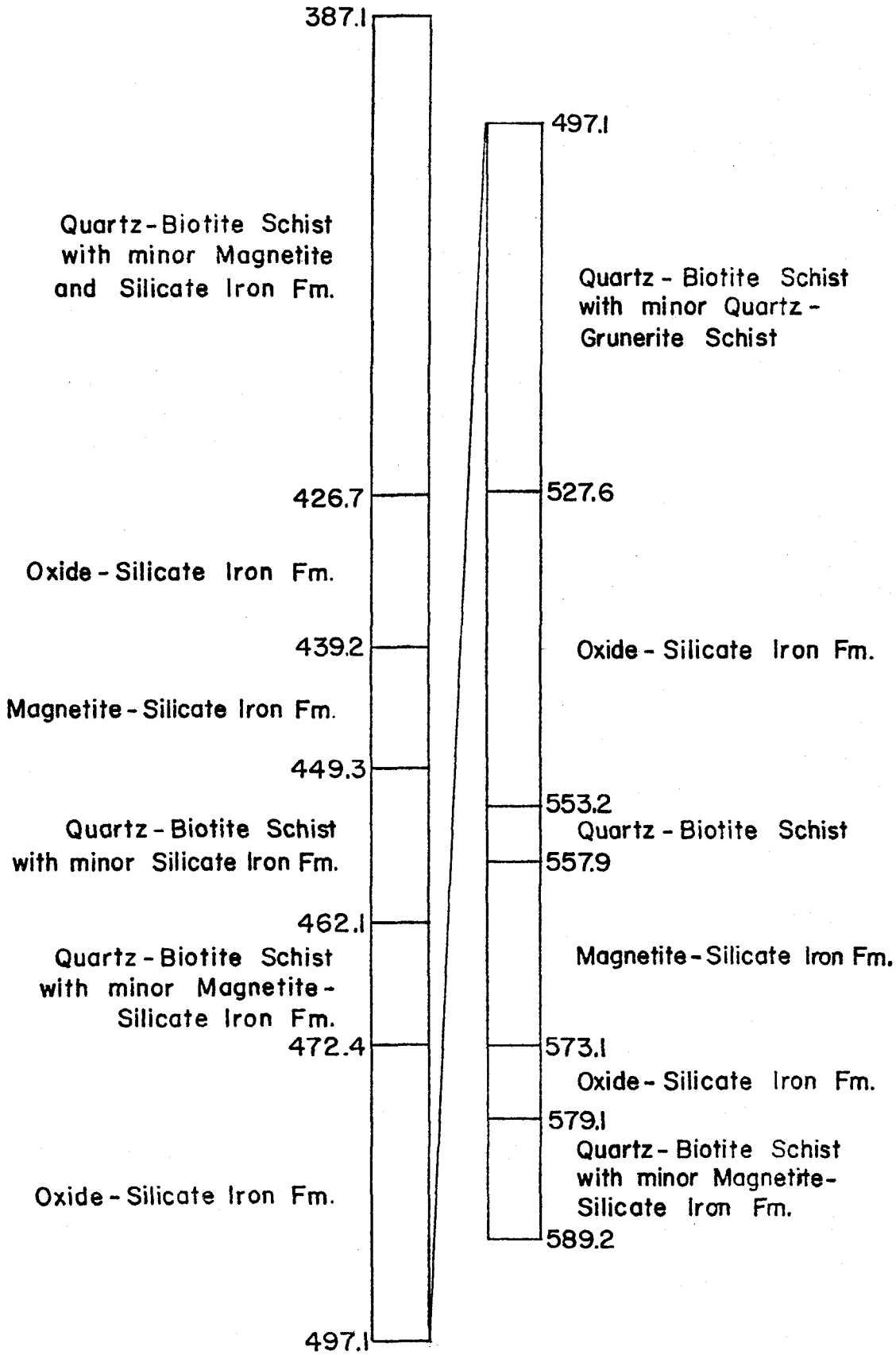
387.1
Quartz-Biotite Schist with minor Magnetite and Silicate Iron Fm.
426.7
Oxide-Silicate Iron Fm.
439.2
Magnetite-Silicate Iron Fm.
449.3
Quartz-Biotite Schist with minor Silicate Iron Fm.
462.1
Quartz-Biotite Schist with minor Magnetite-Silicate Iron Fm.
472.4
Oxide-Silicate Iron Fm.
497.1
497.1
Quartz-Biotite Schist with minor Quartz-Grunerite Schist
527.6
Oxide-Silicate Iron Fm.
553.2
Quartz-Biotite Schist
557.9
Magnetite-Silicate Iron Fm.
573.1
Oxide-Silicate Iron Fm.
579.1
Quartz-Biotite Schist with minor Magnetite-Silicate Iron Fm.
589.2

Fig. 4. Photomicrograph of Quartz-biotite Schist. Bar = 5 mm. Thin Section E70-5.

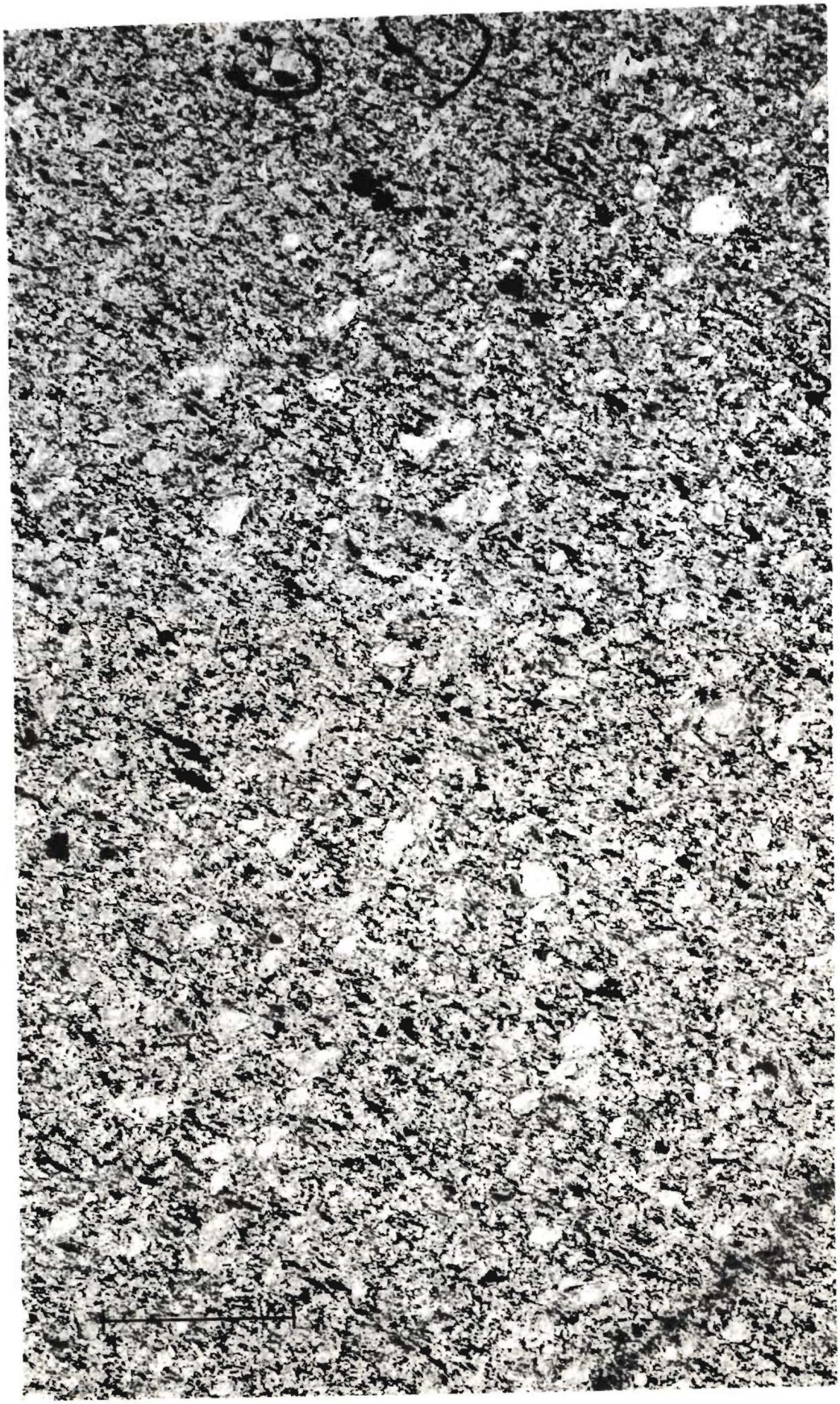

subordinate. A few grains show oscillatory zoning. Subhedral pyrite porphyroblasts, 0.2-0.5 mm, also occur as disseminated grains. In reflected light the grains are brass yellow and isotropic. The grain surfaces are tarnished by application of nitric acid and aqua regia. The other reagents give negative tests. Anhedral magnetite occurs as disseminated grains 0.1-0.2 mm. Anhedral almandite, 1 mm or less, is rare. Alteration products include hematite rimming and replacing magnetite, green chlorite rimming and replacing biotite, and minor sericite after plagioclase.

Magnetite Iron Formation

This fine-grained, gray-black rock consists of fine layers (microbands) about 2 cm or less in thickness (Figure 5). The microbands consist of well-defined, alternating quartz-rich and magnetite-rich laminae a millimetre or less in thickness (Figure 6).

Modal analyses show quartz to range from 40-60 percent, averaging 52 percent. It occurs as anhedral grains 0.02-0.1 mm in diameter. Magnetite ranges from 10-45 percent and averages 28 percent. It occurs as usually anhedral grains which are gray and isotropic in reflected light. Hydrochloric acid and aqua regia solutions turn yellow when applied. The other reagents give negative tests. Some grains show an alteration rim of hematite. Biotite makes up 10-20 percent of the rock. It occurs as subhedral grains, 0.2-0.35 mm, concentrated in the quartz-rich laminae. Anhedral clinozoisite, 0.07-0.14 mm, is usually minor but locally reaches 16 percent. It occurs as both disseminated grains and as veins. Pyrite, 0.2-1.4 percent, occurs mainly as subhedral grains about 0.07 mm in diameter

Fig. 5. Photograph of Magnetite Iron Formation. Bar = 1 cm.

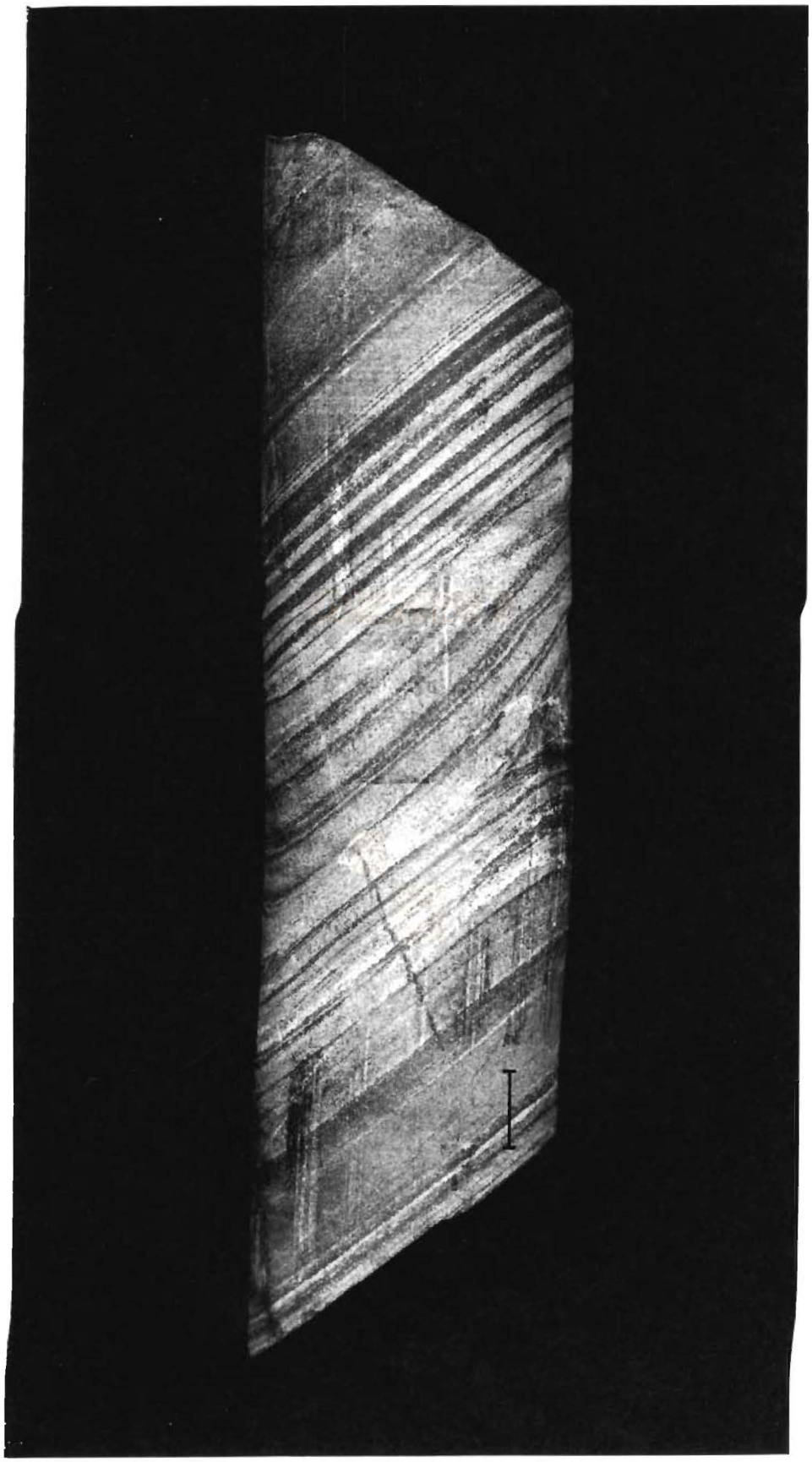

Fig. 6. Photomicrograph of Magnetite Iron Formation. Bar = 5 mm. Thin Section E171-5.

and occasionally as euhedral, cubic porphyroblasts up to 0.5 mm. Plagioclase makes up less than 1 percent of the rock. Subhedral grains, 0.04-0.7 mm, show albite twinning. Pericline and Carlsbad twinning are subordinate. Subhedral sillimanite, .1 mm or less, is occasionally present in minor amounts (less than 1 percent). Anhedral almandite, 1.4 mm or less, is locally abundant (up to 11 percent). Muscovite is a minor constituent of the rock (0.5 percent or less). It occurs as subhedral grains 0.03-0.1 mm.

Magnetite-Silicate Iron Formation

Modal analyses show the rock to average about 57 percent quartz, 11 percent magnetite, 16 percent grunerite, and 11 percent biotite with minor clinozoisite, pyrite, and plagioclase. This thin fine-grained, schistose rock consists of alternating quartz-rich and iron-rich microbands 2 cm or less which are finely laminated on a scale of a millimetre or less. The iron-rich microbands are predominantly magnetite, grunerite, or a combination of the two (Figure 7).

Anhedral quartz, 0.04-0.3 mm, is usually equidimensional. Occasional quartz porphyroblasts reach 0.5 mm. Subhedral grunerite grains, 0.04-0.3 mm, are strongly pleochroic in shades of dark green and light green. The grains show an extinction angle of 10 degrees and an optic axis angle of 85 degrees. The grains are generally subparallel. Grunerite porphyroblasts in coarsely recrystallized zones reach 1.75 mm and many poikilitically enclose quartz. Anhedral magnetite, 0.04-0.2 mm, is concentrated in the iron-rich laminae. Subparallel biotite grains, 0.04-0.5 mm, are concentrated in the quartz-rich layers. Minor clinozoisite, subhedral to euhedral pyrite, and

Fig. 7. Photomicrograph of Magnetite-Silicate Iron Formation. Bar = 5 mm. Thin Section A133-7.

subhedral plagioclase occur in the quartz-rich layers. The plagioclase exhibits albite twinning. Pericline and Carlsbad twinning are subordinate. Subhedral sillimanite grains, .1 mm or less, are rare.

Altered Oxide Iron Formation

This red-green rock consists of 44-50 percent quartz, 1-4 percent magnetite, 22-30 percent hematite, and 15-25 percent chlorite with minor stilpnomelane. The rock is made up of alternating quartz-rich and hematite-rich microbands about 2 cm or less in thickness which are finely laminated on a scale of a millimeter or less. Most range from 0.04-0.35 mm in thickness (Figure 8).

Anhedral, equidimensional quartz grains range from 0.07-0.4 mm. Red earthy hematite grains, 0.07-0.4 mm, have a micaceous habit and occur as subparallel grains. Chlorite occurs as subparallel grains, 0.18-0.35 mm, which are concentrated in the quartz-rich layers. Magnetite, 0.07-0.1 mm, occurs as anhedral grains disseminated in the hematite-rich layers. The grains usually have an alteration rim of hematite. Subhedral stilpnomelane grains, 0.03 mm or less, have a micaceous habit and are pleochroic in shades of pale brown to yellow to light green. The grains show parallel extinction but lack the birdseye mottling characteristic of biotite near the extinction position.

Quartz-Grunerite Schist (Figure 9)

This gray-green rock consists of 52-59 percent quartz, 13-16 percent biotite, 16-24 percent grunerite, 1-11 percent clinozoisite, 0-5 percent magnetite, and accessory plagioclase.

Fig. 8. Photograph of Altered Oxide Iron Formation. Bar = 1 cm.

Fig. 9. Photomicrograph showing Magnetite Iron Formation (Top) and Quartz-Grunerite Schist (Bottom). Bar = 5 mm. Thin Section E260-11.

Equidimensional, anhedral quartz grains occur as fine-grained groundmass, 0.04-0.14 mm, and as porphyroblasts, 0.18-0.88 mm. The porphyroblasts distort surrounding mica and grunerite grains. Grunerite occurs as subhedral grains 0.35-0.88 mm which are usually subparallel but occasionally exhibit rosette structures. Some poikilitically enclose quartz or clinozoisite grains. Biotite, 0.18 mm or less, occurs as subhedral, subparallel grains showing some alteration to green chlorite. Anhedral clinozoisite, 0.18-0.35 mm, occurs as disseminated grains or as veins paralleling or crosscutting schistosity. Anhedral magnetite, 0.03-1 mm, occurs as disseminated grains, some showing alteration rims of hematite. Rare subhedral plagioclase grains (0-0.2 percent) range from 0.1-1 mm and exhibit albite twinning. Pericline and Carlsbad twinning are subordinate. Some grains show oscillatory zoning and some are slightly altered to sericite.

Oxide Iron Formation

This gray-black rock consists of alternating quartz-rich and iron-rich microbands, usually 1 cm or less and finely laminated on a scale from 0.3 mm to 3.5 mm. The iron-rich microbands contain magnetite or magnetite plus specular hematite (Figure 10).

Anhedral quartz, 40-60 percent, occurs as equidimensional grains 0.04-0.2 mm in diameter. Anhedral magnetite grains, 0.18-0.35 mm, make up 20-30 percent of the rock. Subhedral, platy specular hematite grains, 10-14 percent, range from 0.04-0.35 mm. Some grains show a hexagonal outline. In reflected light the grains are steel gray to white and anisotropic. The grains show negative tests to all reagents. Anhedral clinozoisite and subhedral biotite make up less than 5 percent of the rock.

Fig. 10. Photograph of Oxide Iron Formation. Bar = 1 cm.

MINERAL ASSEMBLAGES AND METAMORPHISM

Akra Core

Iron formation in the interval 341.3-463.9 m in the Akra core is characterized by the assemblage quartz-magnetite with biotite, clinozoisite, and minor stilpnomelane, calcite, plagioclase ($Ab_{91}An_9$-$Ab_{90}An_{10}$), pyrite, and muscovite. Quartz-biotite schist in this interval contains quartz-biotite-clinozoisite with minor pyrite and plagioclase ($Ab_{91}An_9$-$Ab_{89}An_{11}$). Rare muscovite is also present. These assemblages are indicative of the greenschist facies of regional metamorphism described by Turner (1968). They are analogous to the biotite subfacies of Huronian iron formation described by James (1955).

Magnetite iron formation below 463.9 m is characterized by the assemblage quartz-magnetite with biotite, clinozoisite, and minor calcite, pyrite, and plagioclase ($Ab_{75}An_{25}$). Magnetite-silicate iron formation in this interval consists of quartz-magnetite-grunerite with biotite, clinozoisite, and minor calcite. Quartz-biotite schist in the interval contains quartz-biotite-clinozoisite with minor magnetite, calcite, and plagioclase ($Ab_{75}An_{25}$). The critical mineral in this interval is grunerite, the key mineral of the amphibolite facies of regional metamorphism of iron formation rocks (James, 1955). The increase in metamorphic grade is also shown by the increased anorthite

content of the plagioclase. Although plagioclase compositions overlap, albite is common in the greenschist facies and oligoclase in the amphibolite facies (Turner, 1968). Biotite, clinozoisite, and calcite persist from greenschist facies through amphibolite facies (James, 1955).

Hensel Core

Magnetite iron formation in the Hensel core contains the assemblage quartz-magnetite with biotite, clinozoisite, calcite, and minor almandite, pyrite, grunerite, sillimanite, and plagioclase ($AB_{80}An_{20}$-$Ab_{75}An_{25}$). Oxide iron formation is characterized by the assemblage quartz-magnetite-specular hematite with minor grunerite, biotite, calcite, and clinozoisite. Magnetite-silicate iron formation contains the assemblage quartz-grunerite-magnetite with biotite, clinozoisite, and some specular hematite. Quartz-biotite schist contains quartz-biotite-clinozoisite with minor magnetite, hematite, grunerite, sillimanite, calcite, pyrite, and plagioclase ($Ab_{80}An_{20}$-$Ab_{75}An_{25}$). The plagioclase becomes more calcic with depth. A few plagioclase grains exhibit oscillatory zoning, a discussion of which is deferred until later. Quartz-grunerite schist is characterized by the assemblage quartz-grunerite-biotite with minor clinozoisite, magnetite, and almandite. Chlorite is present in minor amounts in all of the rock types but is clearly of secondary origin. The mineral assemblages of all of the rock types in the Hensel core are indicative of the amphibolite facies of regional metamorphism as described by Turner (1968) and James (1955).

Magnetite and Oxide Iron Formation

Klein (1973) states that the original, unleached, sedimentary oxide facies of iron formations, as described by James (1955), consist mainly of finely banded mixtures of chert, jasper, or quartz, and magnetite, hematite, or both, and possibly some hydrous iron oxides. French (1973) considers the precursor of the oxide facies to be iron hydroxide with hematite and magnetite as diagenetic products. Both agree that both hematite and magnetite are primary minerals of the oxide facies of unmetamorphosed Precambrian iron formation.

This primary mineralogy persists through greenschist and amphibolite facies of regional metamorphism to yield the quartz-magnetite and quartz-magnetite-specular hematite assemblages observed. No textural evidence was observed that would indicate that these minerals formed at the expense of pre-existing phases or that they reacted to produce new phases. This contradicts Gunderson and Schwartz (1962) who suggested that metamorphism of quartz-magnetite iron formation would produce iron silicates. The quartz-magnetite and quartz-magnetite-specular hematite assemblages are common in metamorphosed iron formations (Klein, 1973). They have been reported from the Biwabik Formation of Minnesota (French, 1968), the metamorphosed Huronian iron formations of northern Michigan (James, 1955), and the Wabush Iron Formation of the Labrador trough (Kranck, 1961).

The persistence of these mineral assemblages through high grade metamorphism indicates that there has been no net gain or loss of oxygen as a result of an externally controlled chemical

potential of oxygen. If movement of oxygen did take place it was sufficiently restricted not to exceed the buffering capacity of the magnetite-specular hematite assemblage or either magnetite or hematite would have been eliminated (Klein, 1973). James (1955) and Klein (1973) consider the recrystallization of chert and iron oxides, resulting in increased grain size, to be the only important effect of metamorphism of oxide facies iron formation. Otherwise, the assemblages persist unchanged through the amphibolite facies.

Silicate Iron Formation

The original silicate facies of iron formation is thought to have consisted of a complex misture of hydrous iron silicates and chert with minor carbonates and iron oxides (Klein, 1973). James (1955) suggested that greenalite is the primary sedimentary silicate and that minnesotaite and stilpnomelane are of low grade metamorphic or diagenetic origin. Whatever the origin, minnesotaite and stilpnomelane persist through the greenschist facies of regional metamorphism.

Upon metamorphism of the silicate facies, complex reactions occur between the silicates and between the silicates and carbonates if any are present (Klein, 1973). Greenalite is replaced by minnesotaite and stilpnomelane in rocks of the greenschist facies (French, 1973). With increasing temperature and pressure to the conditions of the amphibolite facies, pre-existing iron silicates are replaced by grunerite (James, 1955). Iron carbonates react with silica under these conditions as follows:

ferrodolomite + quartz + water = grunerite + calcite + CO_2

siderite + quartz + water = grunerite + orthopyroxene + CO_2

These reactions take place under a low chemical potential of carbon dioxide (Klein, 1973). Biotite, clinozoisite, and calcite persist through amphibolite facies metamorphism (James, 1955).

Quartz-Biotite Schist

The quartz-biotite schist is characterized by the assemblage quartz-biotite-clinozoisite with iron oxides, silicates, calcite, sillimanite, pyrite, and plagioclase. This assemblage is analogous to that found in the fine-grained members of the shale-graywacke suite associated with iron formations in northern Michigan (James, 1955). These are described as silt-sized "graywackes" and shales and resemble the pelitic rocks of the Dalradian and Moine schists of Scotland (James, 1955). Fine-grained schists are typical metamorphic derivatives of pelitic rocks (Hyndman, 1972). Recrystallization leads to poor preservation of original clastic features (James, 1955).

ORIGIN OF GREENSTONE BELTS AND IRON FORMATIONS

Greenstone belts consist of metavolcanic and metasedimentary rocks referred to by Goodwin (1973) as supracrustal assemblages. They typically contain mafic volcanics, felsic pyroclastics, clastic sediments, and iron formations.

Anhaeusser et al. (1969) speculated that the greenstone belts represent discrete depositories and their evolution was controlled by pre-existing structural patterns, the nature of the early crust, and the granites which surround and intrude them as outlined below. The depositional history can be roughly divided into an early magmatic phase and a later sedimentary phase. The earliest event in their evolution was downwarping along fractures in the thin primitive crust. These fractures provided routes for volcanic rocks which formed the initial deposits. The volcanics range in composition from mafic to felsic, with the mafic suite predominating. Pyroclastics and volcanic-derived sediments are commonly intercalated with these rocks. Iron formations may be present in the upper part of the volcanic sequence. The sedimentary phase of deposition may contain a wide range of rock types. Graywackes, shales, and iron formations are characteristic. Conglomerates, breccias, sandstones, and siltstones may also be present.

The iron formations are typically thinly bedded and consist of alternating layers of iron oxides, carbonates, or silicates and

chert (James, 1966). The origin of iron formations has been the subject of much speculation. Even though hypotheses invoking magmatic, volcanic, replacement, and even cosmic processes are still current, most students of iron formation now believe its origin to be as a chemical precipitate (James and Sims, 1973).

There are several problems in this theory. The first problem is concerned with the source of large amounts of iron and silica in solution. James (1966) suggested that the iron and silica are the products of intense chemical weathering of stable low-lying landmasses. He postulated that a higher partial pressure of carbon dioxide in the primitive atmosphere aided weathering and transport of iron and silica. Goodwin (1973), while agreeing with the weathering model for the major iron formations of the middle Huronian, speculated that the common occurrence of earlier iron formations in or near volcanic-rich greenstone belts suggested a genetic link. He attributed the supply of iron and silica to volcanic emanations connected with the evolution of greenstone belts.

The second problem is the banded character of iron formations. The alternating iron-rich and silica-rich layers must be explained in terms of some mechanism which would produce cyclic deposition of iron or silica.

James (1966) postulated that the cyclic deposition was due to the explosive multiplication of silica-secreting organisms in response to periodic increases in either nutrient content or water temperature. He attributed these periodic increases to seasonal variations. Under these conditions iron would precipitate at a constant rate while the

quartz-rich layers would represent periods of organic activity resulting in the precipitation of silica.

Cloud (1973) has pointed out that prokaryotic organisms were dominant in the exclusion of more advanced forms prior to 2 billion years ago. There are no known silica-secreting prokaryotes. Therefore, the banded character of iron formations which were deposited prior to 2 b.y. cannot be explained by James' model. It is questionable whether the model is applicable to any banded iron formation. Cloud (1973) proposed a depositional model in which the atmosphere and hydrosphere were essentially anoxygenous prior to 2 b.y. He cites as evidence for these conditions the extensive deposits of unoxidized, detrital uraninite and pyrite in rocks of that age. Also, terrestrial red beds are uncommon before 2 b.y. Cloud (1973) speculates that there was constant precipitation, under conditions of saturation of the hydrosphere by monosilicic acid, of silica. Photosynthetic oxygen was produced by prokaryotic organisms. This oxygen combined with the iron in solution in the hydrosphere and resulted in the precipitation of iron-rich layers. The cyclic deposition is attributed to the daily fluctuations of photosynthetic activity.

The third problem in explaining the origin of banded iron formations is the restriction of these deposits, with the exception of a few deposits of questionable Cambrian age, to the Precambrian. The principal iron formations of North America are dated at about 2 b.y. (Goldich, 1973). If the primitive atmosphere was in fact anoxygenous, and oxygen was developed by the actions of photosynthetic organisms, the evolution and spreading of these organisms

would contribute more and more oxygen to the atmosphere hampering the transport of iron and silica in solution in surface waters. This could explain why the deposition of iron formations decreases in the late Precambrian and finally ends in the Cambrian.

Precambrian iron formation can be subdivided into geochemical facies on the basis of the chemical elements or compounds with which the iron is combined. The major minerals of the oxide facies are magnetite and hematite. Maghemite (gamma-hematite), a strongly magnetic isometric dimorph of hematite, may also occur (James, 1966). The major mineral of the carbonate facies is siderite. The silicate facies contains greenalite, considered by James (1966) to be a primary silicate, and its metamorphic derivatives; minnesotaite, stilpnomelane, and grunerite. Pyrite and marcasite are the major minerals of the sulfide facies. Pyrrhotite has been reported from sulfide facies iron formation which has been exposed to the high temperatures of contact metamorphism (Gunderson and Schwartz, 1961).

The relationships of the iron compounds are shown by their stability fields in terms of oxidation potential (Eh) and hydrogen ion concentration (pH). The field boundaries are derived from the Nernst equation:

$$Eh = E + \frac{RT}{nF} \ln K$$

where Eh = oxidation potential
E = potential of the reaction
R = universal gas constant
T = Temperature in degrees Kelvin
n = number of electrons involved
F = Faraday constant
lnK = natural log of the equilibrium constant

and from the relation:

$$E = \frac{\Delta F}{nF}$$

where F = change in free energy.

The Eh-pH diagram (Figure 11) represents the range of thermodynamically stable associations possible under specified conditions.

James (1954) related the geochemical facies to water depth and oxygenation in the sedimentary environment of deposition. The oxide facies represents a shallow water environment with high oxygen content; the carbonate facies represents slightly deeper water with a lower oxygen content; the sulfide facies represents deeper stagnant areas where reducing conditions prevail; and the silicate facies, although stable over a wide range of conditions, typically represents areas of weakly oxidizing to weakly reducing conditions. Although no example of all of the facies of Precambrian iron formation grading laterally into one another is known, James (1954) concludes:

> Although it is doubtful if the pattern of precipitation indicated is ever actually obtained in nature because of complicated relationships between depth of basin, height of barrier, and details of circulation, the facies relationships between the various mineralogies are valid.

Fig. 11. Stability Fields of Hematite, Magnetite, and Siderite in Water at 25 Degrees Centigrade, One Atmosphere Total Pressure, and Total Carbonate of 0.01 (After Garrels and Christ, 1965).

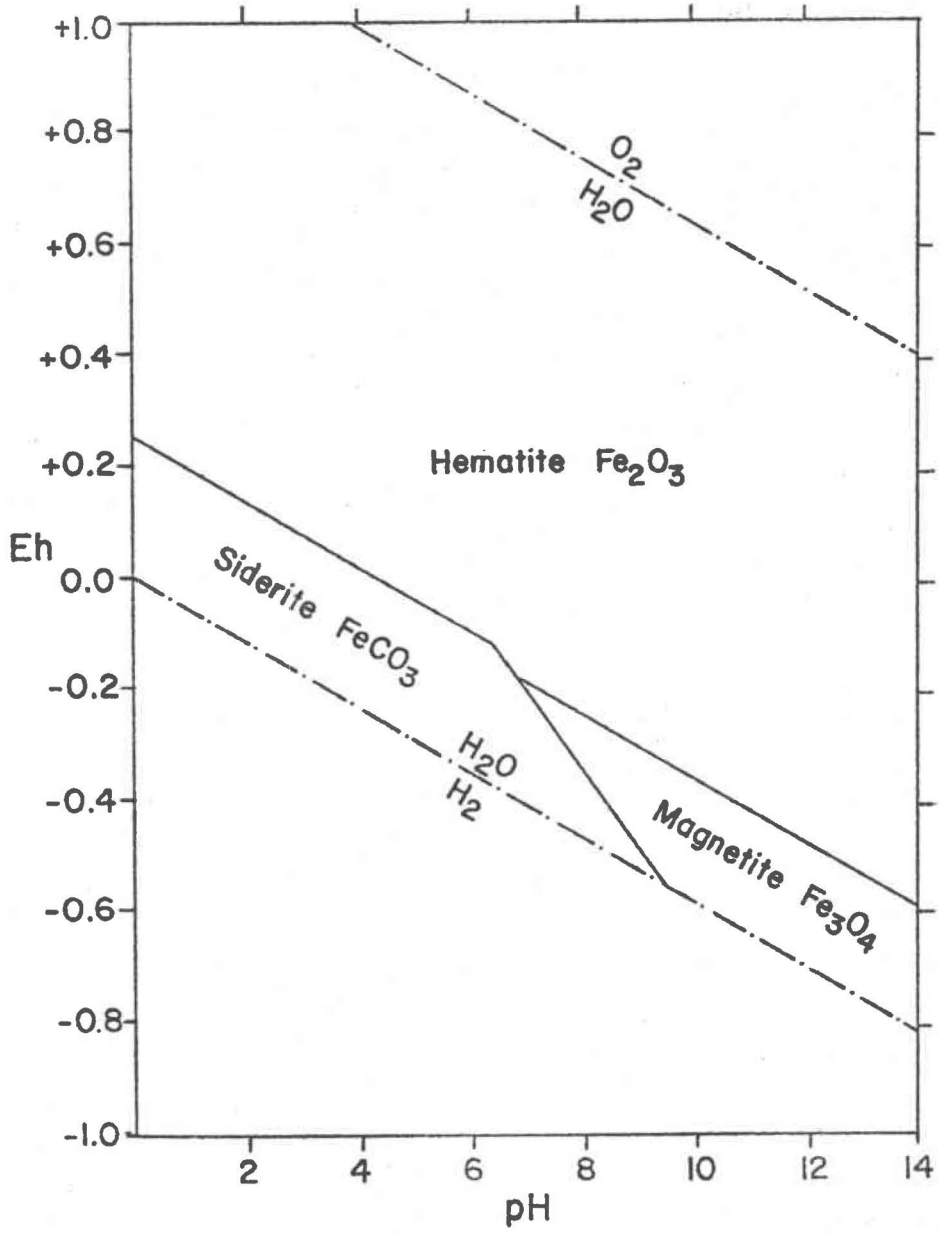
+1.0
+0.8
+0.6
+0.4
+0.2
0.0
-0.2
-0.4
-0.6
-0.8
-1.0
Eh
2
4
6
8
10
12
14
pH
O2
H2O
Hematite Fe2O3
Siderite FeCO3
H2O
H2
Magnetite Fe3O4

INTERPRETATION AND DISCUSSION

The Precambrian rocks of northeastern North Dakota are unconformably overlain by the Ordovician Winnipeg Formation (Anderson, personal communication). They appear to represent the subsurface extension of the Superior Province of the Canadian Shield. The Superior Province is characterized by linear greenstone belts with intervening areas of intrusive, felsic igneous rocks.

Fine-grained actinolite and hornblende schists and gneisses have been reported by Lidiak (in preparation) from greenstone belts of the Precambrian of eastern North Dakota. Lidiak refers to these areas as amphibole schist terranes and states that their predecessors were probably igneous. No rocks of sedimentary origin were reported from the 18 wells which penetrated the amphibole schist terranes. The rocks probably represent the metamorphic derivatives of mafic volcanics of the early magmatic phase of greenstone belt evolution.

The Akra and Hensel rock bodies are located in close proximity to the southwestern termination of one of the amphibole schist terranes mapped by Lidiak (in preparation). The extensions of these belts are imperfectly known. It is likely that the amphibole schist terrane defined by Lidiak in Pembina County could be extended to include the Akra and Hensel sites. It is also probable that the iron formations and interbedded quartz-biotite schists were deposited in the later sedimentary phase of greenstone belt evolution.

The source of iron and silica remains a problem. In many iron formations associated with greenstone belts a close spatial relationship with volcanic rocks can be demonstrated. Lack of control makes it impossible to prove or disprove this relationship for the Akra and Hensel rock bodies. However, the absence of coarse clastic material and the scarcity of volcanic detritus suggest that a period of erosion preceded deposition of the Akra and Hensel rock bodies. Highlands built by earlier volcanism had been largely eroded to low landmasses incapable of supplying coarse debris. Silicate minerals common in volcanic rocks had been largely destroyed by chemical weathering and supplied iron and silica in solution to the basin. When the hydrosphere became saturated with monosilicic acid, silica precipitation began. Iron was cyclically precipitated in response to photosynthetic generation of oxygen by prokaryotic organisms.

Examination of drill cores from the Akra and Hensel rock bodies showed the presence of magnetite, specular hematite, hematite, stilpnomelane, and grunerite. The hematite is secondary and a discussion of its origin is deferred until later. Magnetite and specular hematite represent the oxide facies of Precambrian iron formation. They are deposited in strongly oxidizing to weakly oxidizing conditions respectively. Magnetite is the dominant oxide mineral in both rock bodies. Stilpnomelane and grunerite represent the silicate facies of Precambrian iron formation. The silicate facies is typically deposited in weakly oxidizing to weakly reducing conditions.

The percentages of oxide and silicate minerals in the two cores are plotted against depth in Figures 12 and 13. These show the oxide facies to be dominant in both rock bodies. Silicate minerals are only

Fig. 12. Graph of Iron Oxides and Iron Silicates versus Depth in the Akra Core.

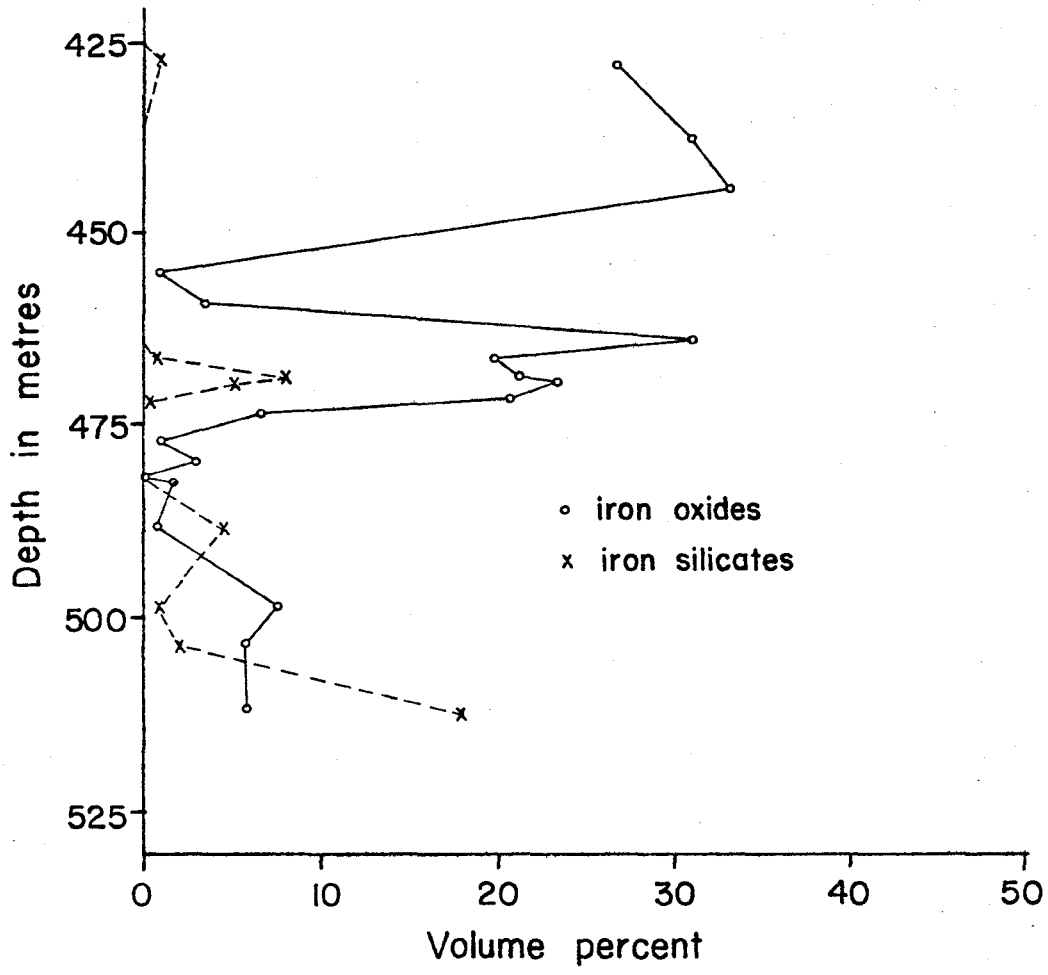
425
450
475
500
525
Depth in metres
iron oxides
iron silicates
0
10
20
30
40
50
Volume percent

Fig. 13. Graph of Iron Oxides and Iron Silicates versus Depth in the Hensel Core.

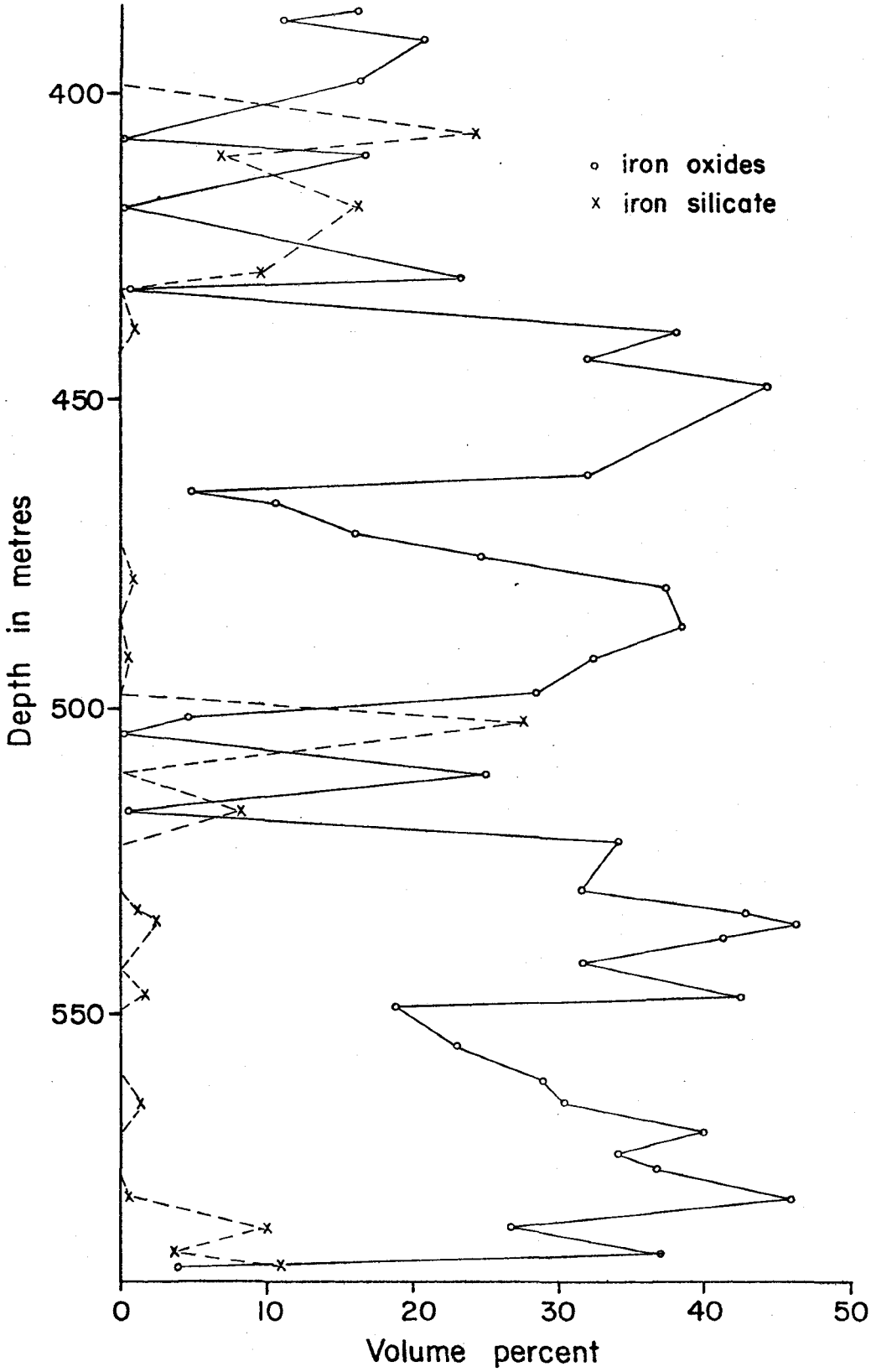
400
450
500
550
Depth in metres
o iron oxides
x iron silicate
0
10
20
30
40
50
Volume percent

locally abundant. This indicates deposition under shallow water conditions. It probably represents later stage basin filling in the sedimentary phase of greenstone belt evolution.

The quartz-biotite schist sequences interbedded with the iron formations are mineralogically and texturally similar to the pelitic rocks associated with iron formations of northern Michigan described by James (1955). These were probably derived from intermittent introduction of fine-grained clastics into the basin. In two zones plagioclase grains exhibiting oscillatory compositional zoning were observed. According to Moorhouse (1959) these can only be formed under igneous conditions and are most likely detrital in origin. Any sedimentary structures which may have been present were destroyed during metamorphism and recrystallization of these fine-grained deposits. This is common in fine-grained rocks subjected to metamorphism (James, 1955). These sequences of interbedded clastic materials might represent periods of structural disturbance in the source areas (James, 1966). During periods of clastic deposition the banded character of iron deposition was interrupted. However disseminated iron oxide and iron silicate grains in the schist sequences show that precipitation continued during these periods.

Age dates from northeastern North Dakota show that the Precambrian rocks of this area were affected by the Laurentian orogeny (2.4-2.75 b.y.). During this period the Hensel and Akra rock bodies were deformed, probably by infolding into the amphibole schist terrane. The general structure of greenstone belts is synformal (Anhaeusser et al., 1969). Higher than normal temperature gradients, possibly due to disturbances in the mantle (Turner and

Verhoogen, 1951) and possibly made more efficient by the nature of the thin crust (Anhaeusser et al., 1969), metamorphosed the rock bodies, the grade of metamorphism increasing with depth.

The upper altered interval in the Akra core contains mainly red, earthy hematite with minor, altered magnetite. The texture of the hematite suggests that it is secondary after specular hematite. It was possibly formed by subaerial weathering or later hydrothermal alteration by ground water. Attributing it to retrograde metamorphism is considered unlikely because it is adjacent to a major unconformity and dies out very quickly with depth. The upper interval of the Hensel core is slightly chloritized but is not severely altered.

With large reserves of near-surface iron ore known in neighboring Minnesota, the depth of the Akra and Hensel rock bodies precludes any present economic consideration. If near-surface reserves become depleted, two intervals in the Hensel rock body are of sufficient thickness and iron oxide content to justify further exploration. These are the intervals from 472.4-497.1 m and 527.6-579.2 m. The iron oxide intervals penetrated in the Akra body are too thin to represent potential ore zones. However the strength of the magnetic anomaly over this body suggests the existence of more extensive bodies at depth.

APPENDIX A

CORE DESCRIPTIONS

OF

AMERADA #1 SIG SAMSON (AKRA)

AMERADA #1 H. SELLHEIM (HENSEL)

Core Description
Amerada #1 Sig Samson
SE¼ Sec. 11, T.161N., R55W.
Ground Level Elevation = 284 m above sea level
Datum is ground level.

Depth in m	Description
423.67-424.28	Alternating hematite and chlorite schist microbands. Microbands are 2 mm or less. Many fractures filled with secondary quartz and calcite. Regular bedding. Dip = 60 degrees. Nonmagnetic.
424.28-425.0	Chlorite schist. Highly altered and very friable. Core badly fractured. Nonmagnetic.
425.0-425.35	Alternating hematite and chlorite schist microbands. Hematite microbands are 10 mm or less. Schist microbands are 6 mm or less. Core badly fractured.
425.35-425.5	Chlorite schist. Nonmagnetic. Core badly fractured.
425.5-430.28	Alternating oxide (mixture of magnetite and hematite) and chlorite schist microbands. The microbands are generally 2 mm or less and are interbedded in zones from 5 to 15 cm. The bedding is highly distorted and dips from 70 to 90 degrees. Modal analysis of thin section A8-2 from this interval showed it to consist of 50% quartz, 3.4% magnetite, 22.8% hematite, 15.4% chlorite, and 8.4% calcite.
430.28-431.29	Chlorite schist. Nonmagnetic.
431.29-431.9	Alternating oxide (2 mm or less) and chlorite schist microbands.
431.9-432.1	Chlorite schist. Nonmagnetic. Core badly fractured.
432.1-435.33	Alternating oxide (2 mm or less) and chlorite schist microbands. Modal analysis of thin section A26-2 from this interval showed it to consist of 44% quartz, 1% magnetite, 29.6% hematite, 25.2% chlorite, and 0.2% calcite.
435.33-439.83	Chlorite schist. Core badly fractured. Nonmagnetic.
439.83-440.74	Finely alternating oxide and chlorite schist microbands. Microbands are 2 mm or less. Regular bedding.

Depth in m	Description
440.74-444.5	Alternating magnetite (2 mm or less) and chlorite schist (6 mm or less) microbands. The bedding is distorted and dips at 80 to 90 degrees. Modal analysis of thin section A44-5 from this interval show it to consist of 43% quartz, 32.8% magnetite, 4.2% biotite, 13.6% chlorite, 1.8% clinozoisite, and 4.4% calcite.
444.5-445.31	Alternating magnetite (1 mm or less) and quartz-biotite schist (6 mm or less) microbands. Bedding mostly regular and dips at about 80 degrees.
445.31-446.18	Quartz-biotite schist. Nonmagnetic.
446.18-447.83	Alternating magnetite (1 mm or less) and schist (3 mm or less) microbands. Bedding mostly regular. Minor disseminated subhedral to euhedral pyrite grains present. Dip = 80 degrees.
447.83-449.88	Quartz-biotite schist. Nonmagnetic.
449.88-451.1	Strongly contorted alternating magnetite and schist microbands. Bedding thickness is irregular. Zones of ptygmatically folded recrystallized quartz present. Minor pyrite occurs as disseminated subhedral grains or as patches of fine anhedral grains. Dip = 80-90 degrees.
451.1-457.12	Quartz-biotite schist. Modal analysis of thin section A87-2 from this interval showed it to consist of 49% quartz, 1% magnetite, 30.8% biotite, and 19.2% clinozoisite. Analysis of X-ray sample XA8-5-19 from this interval showed it to consist of quartz, biotite, chlorite, and minor plagioclase.
457.12-457.5	Strongly folded magnetite and schist microbands. Magnetite microbands are 3 mm or less. Schist microbands are 10 mm or less. Some zones of recrystallized quartz occur as pods or deformed microbands. Pyrite occurs as streaks and patches concentrated at the contacts between different lithologies. Dip = 80 degrees.
457.5-460.12	Quartz-biotite schist. Modal analysis of thin section A98-7 from this interval showed it to consist of 64.4% quartz, 31.8% biotite, 3% magnetite, 0.2% pyrite, 0.2% plagioclase ($Ab_{91}An_9$), and .4% muscovite. Modal analysis of thin section A106-8 from this interval showed it to consist of 60.8% quartz, 18.4% biotite, 17% magnetite, 2.4% clinozoisite, and 1.4% pyrite.

Depth in m	Description
460.12-460.2	Alternating magnetite and schist microbands. Magnetite microbands are 1 mm or less. Schist microbands are 2 mm or less. Dip = 80 degrees.
460.2-460.71	Quartz-biotite schist. Nonmagnetic.
460.71-461.31	Strongly deformed magnetite and schist microbands. Large pods of recrystallized quartz are present and pyrite occurs as disseminated euhedral grains. Modal analysis of thin section A108-1 show it to consist of 35.2% quartz, 33.2% magnetite, 15% biotite, 16% clinozoisite, and 0.6% pyrite. Modal analysis of thin section A110-6 show it to consist of 52% quartz, 25% magnetite, 19.2% biotite, 2.4% clinozoisite, 0.4% pyrite, 0.2% muscovite, and 0.8% plagioclase ($Ab_{91}An_9$).
461.31-461.6	Quartz-biotite schist. Nonmagnetic.
461.6-461.98	Strongly deformed magnetite and schist microbands. The magnetite microbands are 2 mm or less. The schist microbands are 4 mm or less. Minor pyrite occurs as disseminated euhedral grains. Dip varies from 80 to 90 degrees. Modal analysis of thin section A112-5 from this interval show it to consist of 52.4% quartz, 35% magnetite, 11% biotite, 1.4% clinozoisite, and 0.2% pyrite.
461.98-462.38	Quartz-biotite schist. Nonmagnetic.
462.38-467.26	Interbedded magnetite and schist microbands. Microbands are generally 1 mm or less. Some zones of recrystallized quartz are present and associated with some are magnetite microbands up to 4 mm. Some of the magnetite microbands contain minor disseminated euhedral pyrite grains. Modal analysis of thin section 121-10 from this interval show it to consist of 51.8% quartz, 19.8% magnetite, 12.6% biotite, 15% clinozoisite, 0.4% grunerite, and 0.4% calcite. Modal analysis of thin section 130-0 from this interval show it of 61.8% quartz, 14.2% magnetite, 20.4% biotite, 2.4% clinozoisite, 0.2% pyrite, 0.4% muscovite, and 0.6% plagioclase ($Ab_{89}An_{11}$). Analysis of X-ray sample XA13-4-10 showed it to consist of quartz, biotite, clinozoisite, magnetite, and plagioclase.
467.26-472.74	Strongly deformed magnetite, silicate, and schist microbands. Microbands are 6 mm or less. Modal analysis of thin section A131-10 from this interval showed it to consist of 51.4% quartz, 27.2% magnetite,

Depth in m	Description
	2.2% biotite, 9.8% clinozoisite, 8.2% grunerite, and 1.2% calcite. Modal analysis of thin section A132-2 showed it to consist of 61% quartz, 21.4% magnetite, 10% biotite, 9.2% clinozoisite, and 6.8% calcite. Modal analysis of thin section A133-7 showed it to consist of 50.2% quartz, 26.6% magnetite, 5.6% biotite, 9.8% clinozoisite, 6.6% grunerite, and 1.2% calcite. Modal analysis of thin section A134-5 show it to consist of 53.4% quartz, 19.4% magnetite, 3.8% biotite, 10.2% clinozoisite, 4% grunerite, and 9.2% calcite. Modal analysis of thin section A139-11 showed it to consist of 52.6% quartz, 20.6% magnetite, 8.4% biotite, 6.8% clinozoisite, 0.2% grunerite, and 3% calcite.
472.74-473.35	Quartz-biotite schist. Modal analysis of thin section A151-2 show it to consist of 68.4% quartz, 6.4% magnetite, 16.6% biotite, 8.4% clinozoisite, and 0.2% calcite.
473.35-473.96	Strongly deformed magnetite, silicate, and schist microbands. Microbands are 6 mm or less. Dip = 80-90 degrees.
473.96-474.75	Quartz-biotite schist. Nonmagnetic.
474.75-474.93	Magnetite and silicate microbands in schist. Microbands are 3 mm or less. Dip = 80 degrees.
474.93-515.42	Quartz-biotite schist with local concentrations of disseminated magnetite and grunerite grains. Modal analysis of 9 thin sections from this interval showed it to average 62.7% quartz, 3.2% magnetite, 21.5% biotite, 7.6% clinozoisite, 2.9% grunerite, 0.35% calcite, 0.57% pyrite, 0.71% chlorite, and 0.04% plagioclase ($Ab_{75}An_{25}$). Analysis of 7 X-ray samples from this interval showed the same mineralogy.
515.42-515.87	Minor magnetite and very minor silicate microbands in quartz-biotite schist. Some scattered zones of recrystallized quartz present commonly containing concentrations of grunerite porphyroblasts. Minor disseminated grains of pyrite are present.
515.87-529.74	Quartz-biotite schist with minor disseminated magnetite and grunerite grains. Analysis of 5 X-ray samples from this interval showed the mineralogy to consist of quartz, biotite, clinozoisite, magnetite, grunerite, and plagioclase.

Core Description
Amerada #1 H. Sellheim
NE¼ Sec. 8, T.160N., R.54W.
Ground Level Elevation = 274 m above sea level
Datum is Ground Level

Depth in m	Description
387.1-387.6	Magnetite and silicate microbands in schist. Magnetite microbands 1 mm or less. Silicate microbands 2 mm or less. White porphyroblasts of quartz are concentrated in the silicate zones and these zones are slightly magnetic indicating some admixed magnetite. Modal analysis of thin section E1-2 from a magnetite-rich interval show it to consist of 424% quartz, 16.2% magnetite, 2.4% biotite, 12.2% chlorite, 23.4% clinozoisite, 1.8% calcite, and 1.6% plagioclase ($Ab_{80}An_{20}$). Regularly bedded. Dip = 70 degrees.
387.6-388.2	Quartz-biotite schist. Slightly chloritized. Nonmagnetic. Some epidotized fracture surfaces present. Dip = 70 degrees.
388.2-388.3	Minor magnetite microbands (2 mm or less) in schist. Dip = 70 degrees. Some microbands have been offset 1 mm by microfaults. The microfault surfaces have been epidotized.
388.3-388.8	Quartz-biotite schist. Nonmagnetic. Dip = 70 degrees.
388.8-388.9	Magnetite microbands (2 mm or less) alternating with quartz-rich and epidote-rich layers in schist. Dip = 70 degrees.
388.9-388.92	Quartz-biotite schist. Nonmagnetic.
388.92-389.25	Magnetite microbands (2 mm or less) alternating with quartz-rich and epidote rich layers in schist. Modal analysis of thin section E5-9 from this interval showed it to consist of 59.6% quartz, 10.6% magnetite, 5.6% biotite, 9.6% chlorite, 14.6% clinozoisite. Some microbands offset 1 mm by epidotized microfaults. Dip = 70 degrees.
389.25-390.1	Quartz-biotite schist. Nonmagnetic.
390.1-390.15	Finely alternating magnetite and silicate microbands. Dip = 70 degrees.

Depth in m	Description
390.15-391.2	Quartz-biotite schist. Nonmagnetic. Minor epidote microbands 0.5 mm or less parallel bedding. Dip = 70 degrees.
391.2	Slickensided bedding plane fault. Slickensides indicate reverse fault parallelling schistosity. Dip = 70 degrees. Surface of the fault partially covered with secondary calcite. The zone immediately below the fault surface shows some signs of alteration.
391.2-391.24	Altered silicate and magnetite microbands. The silicate microbands show some signs of chloritization and the magnetite is partially altered to hematite.
391.24-391.5	Magnetite and silicate microbands in schist. Slight alteration of magnetite to hematite. Some augen structures of slightly altered green silicates are present in the magnetite microbands. These are elongate parallel to schistosity, the long axis of the largest being 1 cm and its short axis about 2 mm. The zone is transected by a fracture surface dipping at about 80 degrees. The fracture surface is partially covered with secondary calcite.
391.5-391.77	Quartz-biotite schist. Nonmagnetic. Core badly fractured.
391.77	Epidotized slickensided high angle fault. Dip of fault plane about 75 degrees. Slickensides indicate normal faulting with a component of lateral movement at about 45 degrees to the dip of the schistosity.
391.77-392.28	Quartz-biotite schist. Nonmagnetic. Some minor epidote veins are present. Some parallel and others transect schistosity. White porphyroblasts of quartz are present in the schist and there is minor garnet present.
392.28-392.38	Fracture zone in altered quartz-biotite schist containing minor magnetite microbands. The magnetite shows signs of alteration to hematite and the schist shows signs of chloritization. Modal analysis of thin section E26-6 from the magnetite-rich zone shows it to consist of 44.8% quartz, 19.8% magnetite, 0.2% hematite, 22.4% epidote, 10.2% calcite, and 2.6% garnet. The fracture surfaces appear to be mylonitized.
392.38-392.76	Quartz-biotite schist with some epidote and calcite veins. Nonmagnetic.

Depth in m	Description
392.76-392.96	Magnetite and silicate microbands in quartz-biotite schist.
392.96	Fracture surface parallelling schistosity. Dip = 70 degrees. The fracture surface is covered with secondary calcite. At 1 mm zone of altered schist occurs on each side of the fracture.
392.96-393.85	Zone of badly fractured quartz-biotite schist. Nonmagnetic.
393.85-394.4	Quartz-biotite schist.
394.4	Epidotized slickensided fault surface. Fault dip direction nearly perpendicular to dip of schistosity. Fault surface partially covered with secondary calcite.
394.4-394.54	Quartz-biotite schist. Nonmagnetic.
394.54-394.55	Magnetite microband. Dip = 70 degrees.
394.55-394.72	Quartz-biotite schist. Nonmagnetic.
394.72-395.15	Magnetite and silicate microbands in quartz-biotite schist. Bedding mostly regular but some microbands are contorted. Some silicate augen structures present. Garnet augens rimmed with epidote are also present. Dip = 70 degrees.
395.15-395.33	Epidotized quartz-biotite schist. Nonmagnetic. Minor silicate microbands containing quartz porphyroblasts are present. Dip = 70 degrees.
395.33-395.94	Badly fractured, epidotized magnetite microbands in quartz-biotite schist. Fracture surfaces epoditized and slickensided. Garnet augens present in some magnetite microbands.
395.94-396.26	Minor silicate and magnetite microbands in quartz-biotite schist. Minor epidote veins are present. Some parallel and others transect schistosity which dip at 70 degrees.
396.26-396.44	Quartz-biotite schist with minor epidote veins. Nonmagnetic.
396.44-396.45	Recrystallized quartz zone parallelling schistosity. Dip = 70 degrees. Patches of silicate, epidote, and garnet occur in the quartz. The upper and lower contact of the quartz with the adjacent quartz-biotite schist is marked by epidote zones about 0.5 mm

Depth in m	Description
	thick. The quartz zone is also transected by minor epidote veins.
396.45-397.21	Quartz-biotite schist. Nonmagnetic.
397.21	Epidotized, slickensided fracture surface dipping at 70 degrees and transection schistosity. Slickensides indicate a high angle reverse fault.
397.21-397.36	Quartz-biotite schist. Nonmagnetic.
397.36-398.37	Magnetite and minor silicate microbands in quartz-biotite schist. Modal analysis of thin section E37-6 from this interval showed it to consist of 66% quartz, 15% magnetite, 0.8% hematite occuring as alteration rims on magnetite grains, 5.8% biotite, 8.4% clinozoisite, 0.2% calcite, and 0.2% plagioclase ($Ab_{80}An_{20}$). Bedding mostly regular, some contorted. Dip = 70 degrees.
398.37-398.98	Quartz-biotite schist. Nonmagnetic.
398.98-400.66	Quartz-biotite schist with very minor magnetite and silicate microbands.
400.66-401.29	Magnetite and silicate microbands in quartz-biotite schist. Regularly bedded. Some microbands offset 1 mm by microfaults. Dip = 70 degrees.
401.29-401.52	Quartz-biotite schist. Some quartz porphyroblasts present. Nonmagnetic.
401.52-403.86	Quartz-biotite schist with minor epidote and associated garnet. Dip = 70 degrees. Epidote occurs as veins (1-2 mm) parallelling schistosity. The garnet occurs as zones (2-3 mm) at the contacts between the epidote veins and the quartz-biotite schist.
403.86	Slickensided bedding plane fault.
403.86-404.1	Badly fractured, altered quartz-biotite schist. The pieces appear to be slickensided and serpentinized. The schist has been chloritized.
404.1-404.34	Quartz-biotite schist. Nonmagnetic.
404.34	Epidotized fracture surface parallelling schistosity. Dip = 70 degrees.

Depth in m	Description
404.34-406.0	Fractured, unaltered quartz-biotite schist. Non-magnetic.
406.0	Epidotized, slickensided fault parallelling schistosity. Movement parallelled strike of schistosity. Dip = 70 degrees.
406.0-407.8	Fractured quartz-biotite schist with disseminated silicate grains. Some development of epidote veins with associated garnet. Modal analysis of thin section E70-5 from this interval showed it to consist of 52.2% quartz, 15.4% biotite, 1.0% clinozoisite, 23.8% grunerite, and 7.4% plagioclase ($Ab_{75}An_{25}$).
407.8-409.0	Quartz-biotite schist. Nonmagnetic. Some fine-grained pyrite present. Also contains minor epidote veins.
409.0-410.37	Quartz-biotite schist with minor magnetite and silicate microbands.
410.37-410.57	Magnetite and minor silicate microbands in quartz-biotite schist. Microbands 3 mm or less. Bedding regular. Dip = 65 degrees. Modal analysis of thin section E79-8 from this interval showed it to consist of 56.8% quartz, 16.8% magnetite, 12.4% biotite, 6.0% clinozoisite, 7.8% grunerite, .2% plagioclase ($Ab_{75}An_{25}$), and 0.2% sericite occurring as an alteration product of plagioclase.
410.57-410.97	Moderately fractured quartz-biotite schist with some epidite veins.
410.97-412.4	Magnetite and silicate microbands in quartz-biotite schist. Magnetite microbands 1 mm or less. Silicate microbands 1.5 mm or less. Some microbands offset 0.5 mm by microfaults. Dip = 65 degrees.
412.4-412.85	Quartz-biotite schist with minor silicate microbands. Nonmagnetic.
412.85-413.0	Magnetite and some silicate microbands in quartz-biotite schist. Bedding mostly regular, some slightly contorted. Some augen structures of epidote present and also traces of garnet.
413.0-413.41	Quartz-biotite schist. Nonmagnetic.
413.41-413.46	Magnetite and some green silicate microbands in quartz-biotite schist.

Depth in m	Description
413.46-413.7	Quartz-biotite schist. Nonmagnetic.
413.7-413.92	Magnetite and silicate microbands in quartz-biotite schist. Some garnet and epidote veins paralleling schistosity. Dip = 70 degrees.
413.92-414.43	Quartz-biotite schist with minor epidote and garnet.
414.43-414.63	Minor magnetite and silicate microbands in quartz-biotite schist. Abundant epidote present.
414.63-415.27	Quartz-biotite schist. Nonmagnetic.
415.27	Possible bedding plane fault.
415.27-415.62	Minor magnetite and silicate microbands in quartz-biotite schist. Minor epidote present.
415.62-416.1	Quartz-biotite schist with secondary quartz and epidote veins. Nonmagnetic.
416.1-416.23	Magnetite and silicate microbands in quartz-biotite schist. Dip = 70 degrees.
416.23-416.67	Quartz-biotite schist with minor epidote. Nonmagnetic. Dip = 70 degrees.
416.67-416.71	Magnetite and minor silicate microbands in schist. Microbands 2 mm or less. Regularly bedded. Dip = 70 degrees.
416.71-418.59	Quartz-biotite schist with minor magnetite microbands.
418.59	Epidotized, slickensided high angle fault. Dip = 80 degrees. Normal fault with some horizontal movement.
418.59-421.77	Quartz-biotite schist with minor, scattered oxide and silicate microbands. Dip = 70 degrees. Modal analysis of thin section E111-1 from a silicate-rich zone showed it to consist of 59.2% quartz, 16% biotite, 2.2% clinozoisite, 16% grunerite, and 6.6% plagioclase ($Ab_{75}An_{25}$). Analysis of X-ray sample XE12 from the schist showed it to consist of quartz, biotite, clinozoisite, magnetite, and plagioclase.
421.77	Epidotized, slickensided high angle fault paralleling schistosity.
421.77-422.45	Quartz-biotite schist. Nonmagnetic.

Depth in m	Description
422.45-423.67	Quartz-biotite schist with minor garnet. Nonmagnetic.
423.67-426.1	Fractured quartz-biotite schist with minor magnetite and silicate microbands. Fracture surfaces are epidotized and some show weakly developed slickensides. Analysis of X-ray sample XE13 from this interval showed it to consist of quartz, biotite, grunerite, magnetite, clinozoisite, and plagioclase.
426.1-426.72	Minor magnetite microbands in slightly to nonmagnetic quartz-biotite schist. Magnetite microbands 2 mm or less. Schist contains abundant epidote. Core badly fractured. Some pieces show spidotized, slickensided surfaces. Dip = 70 degrees.
426.72-427.0	Magnetite and silicate microbands in schist. Magnetite microbands 3 mm or less. Silicate microbands 1 mm or less. Dip = 70 degrees.
427.0-433.8	Core badly broken. Specular hematite, magnetite, and silicate microbands in schist. Oxide microbands 6 mm or less. Silicate microbands 6 mm or less. Silicate grains and epidote are also disseminated in the quartz-biotite schist zones. Some oxides occur in the silicate microbands. Some silicate microbands also exhibit pinch and swell structures. Areas of coarsely recrystallized quartz are common. Some core fragments show epidotized fracture surfaces, some of which exhibit slickensides. The majority of these fractures parallel schistosity but some transect it. Minor chalcopyrite is developed on one fracture surface at 42.78 m. There is a spotty development of garnet, usually associated with epidote. Modal analysis of thin section E140-5 from this interval showed it to consist of 46.8% quartz, 17% magnetite, 5.4% specular hematite, 5.2% chlorite, 13.2% clinozoisite, 9.8% grunerite, and 1.8% plagioclase ($Ab_{75}An_{25}$). Modal analysis of thin section E149-11 from a schist zone in this interval showed it to consist of 58.8% quartz, 0.2% magnetite, 32.4% biotite, 4.2% clinozoisite, and 4.4% plagioclase of the same composition as that in thin section E140-5. Analysis of X-ray sample XE15 from this interval showed it to consist of quartz, magnetite, hematite, and clinozoisite.
433.8-434.5	Core badly fractured. Magnetite microbands and silicate microbands with minor epidote interlayered with quartz-biotite schist. Magnetite microbands 4 mm or less. Silicate microbands 2 mm or less. Some pieces show epidotized, slickensided fracture surfaces.

Depth in m	Description
434.5-434.64	Specular hematite, magnetite, and silicate microbands with minor schist. Core badly fractured.
434.64-435.25	Core badly fractured. Quartz-biotite schist. Non-magnetic. Minor epidote veins crosscut schistosity. A few pieces show epidotized fracture surfaces, some with poorly developed slickensides.
435.25-435.45	Magnetite and specular hematite microbands interlayered with quartz-biotite schist. Specular hematite microbands 4 mm or less. Magnetite microbands 1.5 mm or less. Dip = 60 degrees. Analysis of X-ray sample XE17 showed the oxide zones to consist of quartz, magnetite, and hematite.
435.45-436.8	Magnetite and specular hematite microbands and silicate microbands (coarse-grained) interlayered with quartz-biotite schist. Some microbands offset 1 mm of less by a series of parallel epidotized microfaults. The microfaults transect schistosity and dip at about 80 degrees. Some pieces show epidotized, slickensided fracture surfaces with very coarse-grained epidote developed on some of the fracture surfaces. Dip = 70 degrees.
436.8-437.54	Quartz-biotite schist with very minor magnetite microbands (6 mm zone). Some secondary quartz filling fractures.
437.54-437.99	Magnetite, specular hematite, and silicate microbands interlayered with quartz-biotite schist. Magnetite microbands are more common near the top of the interval and specular hematite microbands near the bottom. Grunerite crystals form random felted patterns on some rock cleavage surfaces. Core badly fractured. Some pieces exhibit epidotized, slickensided fracture surfaces.
437.99-438.6	Magnetite and specular hematite microbands interlayered with quartz-biotite schist. Silicate microbands minor. Microbands 1 mm or less. Dip = 70 degrees. Modal analysis of thin section E171-5 from this interval showed it to consist of 55.8% quartz, 26% magnetite, 11.4% specular hematite, 1.8% clinozoisite, 0.6% grunerite, and 1.6% calcite.
438.6-439.37	Magnetite and specular hematite microbands interlayered with quartz-biotite schist. Iron oxide microbands 2 mm or less. Dip = 70 degrees. Some epidotized fracture surfaces present.

Depth in m	Description
439.37-439.9	Quartz-biotite schist. Nonmagnetic.
439.9	Fault transection schistosity. Dip = 40 degrees.
439.9-440.38	Quartz-biotite schist. Nonmagnetic.
440.38-440.45	Magnetite, silicate, and minor epidote microbands interlayered with quartz-biotite schist. Magnetite microbands 4 mm or less. Silicate microbands 2 mm or less. Dip = 65 degrees.
440.45	Fault. Transects schistosity and dips at 60 degrees.
440.45-440.74	Magnetite, silicate, and minor epidote microbands interlayered with quartz-biotite schist. Dip = 65 degrees.
440.74-441.58	Quartz-biotite schist with minor epidote. Dip = 60 degrees.
441.58-445.67	Magnetite and silicate microbands in quartz-biotite schist. Magnetite microbands 4 mm or less. Silicate microbands 2 mm or less. Quartz porphyroblasts present in some magnetite microbands. Epidote-rich microbands exhibit pinch and swell structure. Some of these structures have developed to the point that they occur at discontinuous lenses. Coarse-grained quartz fills some secondary fractures. Modal analysis of thin section E187-8 from a magnetite-rich zone in this interval showed it to consist of 64.6% quartz, 29% magnetite, 2.6% hematite, 1.6% clinozoisite, 1.4% calcite, 0.6% biotite, and 0.2% chlorite.
445.67-446.23	Quartz-biotite schist with a minor zone of magnetite microbands. Modal analysis of thin section E196-8 from the iron-rich zone showed it to consist of 36.8% quartz, 43.6% magnetite, 0.2% hematite, 11.8% biotite, 0.8% chlorite, and 6.8% clinozoisite.
446.23-446.53	Magnetite and silicate microbands interlayered with quartz-biotite schist. One minor specular hematite microband occurs at 446.34 m. Core badly broken. Some pieces show epidotized, slickensided fracture surfaces transecting schistosity and dipping at about 80 degrees. Minor chalcopyrite developed on one fracture surface.
446.53-447.59	Quartz-biotite schist with minor, widely spaced magnetite microbands. Quartz porphyroblasts locally abundant in the schist. Dip = 60 degrees.

Depth in m	Description
447.59-447.75	Closely spaced magnetite microbands interlayered with quartz-biotite schist and silicate microbands. Silicates occur as individual microbands or as porphyroblasts in the magnetite microbands. Microbands 4 mm or less. Dip = 60 degrees.
447.75-448.67	Quartz-biotite schist with locally abundant quartz porphyroblasts. Nonmagnetic.
448.67-449.0	Magnetite and silicate microbands interlayered with quartz-biotite schist. Lower 17 cm of the interval badly fractured. The fracture surfaces are epidotized and some show poorly developed slickensides. Fractures transect schistosity and dip at about 60 degrees.
449.0-462.1	Quartz-biotite schist interlayered with minor silicate microbands. White quartz porphyroblasts locally abundant in both the schist and the silicate microbands. Core is locally badly fractured and some fracture surfaces are epidotized and exhibit slickensides. Fracture surfaces both parallel and transect schistosity. Minor pyrite grains occur in the quartz-biotite schist. Analyses of 3 X-ray samples from this interval showed it to consist of quartz, biotite, clinozoisite, magnetite, grunerite, and plagioclase.
462.1-462.51	Magnetite and silicate microbands interlayered with quartz-biotite schist. Abundant epidote associated with the silicate microbands. Mostly regularly bedded but the zone from 464.23 m to 462.46 m is strongly folded. Some of the microbands in this zone have been pulled apart and broken up. Garnet pods are present in the quartz-biotite schist. Magnetite and silicate microbands are 4 to 5 mm or less. Dip = 65 degrees. The strongly folded zone possibly represents a shear zone. Modal analysis of thin section E254-2 from a magnetite-rich zone in this interval showed it to consist of 41.6% quartz, 31.2% magnetite, 0.2% hematite, 12.2% biotite. 5.6% chlorite, 9% clinozoisite, and 0.2% pyrite.
462.51-462.92	Quartz-biotite schist with some silicate microbands.
462.92-463.35	Magnetite and silicate microbands interlayered with quartz-biotite schist. Abundant epidote associated with the silicate microbands. It also occurs as zones between silicate and magnetite microbands. Strongly contorted bedding in the interval from 463.0 to 463.17 m may represent a shear zone.

Depth in m	Description
463.35-463.96	Quartz-biotite schist with very minor magnetite microbands (.5 mm or less). Regularly bedded. Dip = 60 degrees.
463.96-464.21	Magnetite and silicate microbands interlayered with quartz-biotite schist. Magnetite microbands 2 mm or less. Silicate microbands 7 mm or less. Regularly bedded. Dip = 60 degrees. Quartz porphyroblasts 1 mm or less are concentrated in some of the silicate microbands and are elongated parallel to schistosity. Minor zones of coarsely recrystallized quartz and magnetite are present. Some minor cross-cutting quartz and epidote veins also occur. Modal analysis of thin section E260-11 from a schist zone in this interval showed it to consist of 41% quartz, 4.6% magnetite, 10.4% biotite, 10.2% chlorite, 30.6% clinozoisite, 2.4% calcite, and 0.8% plagioclase ($Ab_{75}An_{25}$).
464.21-465.35	Quartz-biotite schist with one minor (6 mm) zone of silicate microbands occurring at 464.57 m. Quartz porphyroblasts 2 mm or less are common in the schist. Minor pyrite is also present.
465.35-465.96	Magnetite and silicate microbands with minor quartz-biotite schist. Magnetite and silicate microbands 3 mm or less. Minor euhedral pyrite grains (1 mm or less) present. Dip = 60 degrees. Modal analysis of thin section E265-3 from a magnetite-rich zone in this interval showed it to consist of 65% quartz, 10% magnetite, .2% hematite, .2% clinozoisite, 13.6% calcite, and 11% almandite.
465.96-468.17	Quartz-biotite schist. Quartz porphyroblasts common. Dip = 60 degrees. Nonmagnetic.
468.17-468.84	Quartz-biotite schist with minor (.5 mm or less) widely spaced magnetite microbands. Minor pyrite present in both the schist and the magnetite microbands.
468.84-468.99	Quartz-biotite schist with minor magnetite and silicate microbands. Core badly fractured. Fracture surfaces epidotized and slickensided. Microbands strongly deformed.
468.99-470.92	Quartz-biotite schist with abundant quartz porphyroblasts. Minor epidote veins paralleling schistosity are present. Nonmagnetic.

Depth in m	Description
470.92	Epidotized fracture surface transecting schistosity and dipping at 85 degrees.
470.92-471.83	Quartz-biotite schist with minor magnetite and silicate microbands. Magnetite microbands 1 mm or less. Silicate microbands 2 mm or less. Dip = 55 degrees.
471.83-472.14	Magnetite and minor silicate microbands interlayered with quartz-biotite schist. Microbands 4 mm or less. Dip = 55 degrees. Modal analysis of thin section E286-7 from this interval showed it to consist of 43.6% quartz, 15.8% magnetite, .2% biotite, 14.8% chlorite, 24.8% clinozoisite, and .8% plagioclase ($Ab_{75}An_{25}$).
472.14-472.24	Fracture zone in magnetite and silicate microbands. Fracture surfaces epidotized and slickensided.
472.24-472.39	Quartz-biotite schist. Nonmagnetic.
472.39-472.44	Magnetite microbands in schist. Microbands .55 mm or less. Dip = 60 degrees.
472.44-497.13	Magnetite and specular hematite microbands alternating with quartz-biotite schist. Core badly broken. Bedding mostly regular but some zones show complex folding suggestive of bedding plane slippage. Silicate porphyroblasts are common in the schist zones and usually parallel schistosity. Minor pyrite occurs in the interval both as disseminated grains and as concentrations on fracture surfaces. The pyrite grains range from euhredral to anhedral. The oxide microbands are generally less than 2 mm but occasionally reach 10 mm. Schist zones are generally less than 2.5 cm. Modal analyses were performed on five thin sections from this interval and showed it to average 55.3% quartz, 23.9% magnetite, 7.9% specular hematite, 0.4% biotite, 5.6% chlorite. 4.1% calcite, 0.1% grunerite, 1.5% clinozoisite, and 0.2% muscovite. These mineralogies were verified by analyses of 2 X-ray samples which also showed the presence of plagioclase.
497.13-497.89	Quartz-biotite schist with minor magnetite and wilicate microbands. Microbands are less than 2 mm. Regularly bedded. Dip = 60 degrees.
497.89-499.47	Strongly contorted magnetite and silicate microbands in quartz-biotite schist. Silicate porphyroblasts are present in some schist zones and reach up to 4 mm in length. Most parallel schistosity but some

Depth in m	Description
	porphyroblast-rich areas exhibit random orientation of the silicate grains. Minor euhedral pyrite is present.
499.47-500.48	Quartz-biotite schist with plagioclase porphyroblasts. Nonmagnetic. Dip = 60 degrees.
500.48-502.92	Quartz-grunerite schist with minor magnetite and silicate microbands. Anhedral pyrite occurs as disseminated anhedral grains and as concentrations in pods of recrystallized quartz. Modal analysis of thin section E387-2.5 from this interval showed it to consist of 51.6% quartz, 4.4% magnetite, 12.6% biotite, 2.6% clinozoisite, 27.2% grunerite, 0.4% calcite, .4% pyrite, and 0.8% almandite. Analysis of X-ray sample XE39 showed the presence of quartz, grunerite, clinozoisite, and bavalite.
502.92-527.61	Quartz-biotite schist with very minor magnetite and silicate microbands. Iron-rich zones are generally less than 4 mm but occasionally reach 35 mm. Dip = 40 degrees. Silicate porphyroblasts generally parallel schistosity but some exhibit random orientation. This is especially common at the contacts between magnetite and schist zones. Pyrite enrichment is also common at these sites. The pyrite occurs as anhedral disseminated grains. Modal analysis of thin section E401-5 from a schist zone in this interval showed it to consist of 64.2% quartz, 33.8% biotite, 0.8% clinozoisite, .8% pyrite, 0.2% pyrite, and 0.2% plagioclase ($Ab_{75}An_{25}$). Modal analysis of thin sections E422-10 and E457-4 from magnetite-rich zones in this interval showed them to average 43% quartz, 29.3% magnetite, 0.9% biotite, 15.4% chlorite, 10% clinozoisite, 1% calcite, and 0.3% pyrite. Modal analysis of thin section E443-6 from a silicate zone in this interval showed it to consist of 76.4% quartz, .2% magnetite, 2.8% biotite, 6.4% clinozoisite, 8.2% grunerite, 4.4% caccite, 0.2% oligoclase, and 1.4% sillimanite.
527.61-553.21	Magnetite, specular hematite, and silicate microbands in schist. The microbands are 8 mm or less. Bedding ranges from regular to highly contorted. Minor disseminated pyrite occurs as euhedral grains and as clusters of anhedral grains. The contorted zones commonly contained pods of recrystallized quartz. Minor garnet is present at 533.4 m. Modal analyses of 6 thin sections from this interval showed it to average 53.7% quartz, 33.4% magnetite, 1.75% hematite,

Depth in m	Description
	3.7% biotite, 1.4% chlorite, 1.2% clinozoisite, 1% grunerite, 3.5% calcite, and 0.1T oligoclase.
553.21-557.94	Quartz-biotite schist with minor magnetite microbands. Magnetite microbands 2 mm or less. Dip = 30 degrees. Modal analysis of thin section E570-4 from an iron-rich zone in this interval showed it to consist of 46.2% quartz, 22.6% magnetite, 21% biotite, 3.2% chlorite, 0.6% clinozoisite, and 4.6% calcite.
557.94-558.52	Magnetite and silicate microbands interlayered with quartz-biotite schist. Magnetite microbands 3 mm or less. Silicate microbands 20 mm or less. Bedding mostly regular except for a strongly contorted zone from 558.30-558.39 m. Dip = 20 degrees. Modal analysis of thin section E588-5 from a magnetite-rich zone in this interval showed it to consist of 39.2% quartz, 28.6% magnetite, 0.2% hematite, 9% biotite, 0.2% chlorite, 8.8% clinozoisite, 1% calcite, and 0.2% oligoclase.
558.52-559.26	Silicate microbands and very minor, scattered magnetite microbands in quartz-biotite schist. Silicate microbands 25 mm or less. Bedding regular. Dip = 60 degrees.
559.26-559.31	Highly contorted magnetite and silicate microbands in quartz-biotite schist.
559.31-559.41	Magnetite and very minor silicate microbands interlayered with quartz-biotite schist. Magnetite microbands 2 mm or less. Schist zones 5 mm or less. Bedding regular to slightly contorted. Dip = 30 degrees.
559.41-561.26	Nonmagnetic quartz-biotite schist with some silicate microbands. Scattered augen-shaped pods of recrystallized quartz with traces of garnet present.
561.26-561.44	Magnetite and silicate microbands in schist. Magnetite microbands 2 mm or less. Silicate microbands 15 mm or less. Silicate microbands are slightly magnetic. Regularly bedded. Dip = 30 degrees.
561.44-561.66	Quartz-biotite schist. Nonmagnetic.
561.66-565.4	Magnetite and silicate microbands interlayered with slightly to nonmagnetic quartz-biotite schist. Some pods of recrystallized quartz (some rimmed by epidote) containing traces of pyrite and garnet are present. Bedding regular to slightly contorted. Dip = 25 degrees. Modal analysis of thin section E604-8 from

Depth in m	Description
	this interval showed it to consist of 54.8% quartz, 28.8% magnetite, 0.2% hematite, 3% biotite, 4.6% clinozoisite, 1.6% grunerite, and 7% calcite.
565.4-567.28	Nonmagnetic quartz-biotite schist with some silicate microbands. Some contorted areas show concentrations of recrystallized quartz, epidote, and garnet.
567.28-567.79	Magnetite and silicate microbands in schist. Magnetite microbands 10 mm or less. Silicate microbands 5 mm or less. Bedding distorted and discontinuous.
567.79-568.55	Quartz-biotite schist with minor magnetite microbands. Bedding regular to slightly contorted. Sulfides occur as euhedral grains and as fine-grained masses of anhedral grains.
568.55-568.76	Magnetite and silicate microbands interlayered with schist microbands. Magnetite microbands 2 mm or less. Silicate microbands 5 mm or less. Schist microbands 10 mm or less. Minor pyrite occurs as euhedral, cubic crystals. Minor epidote occurs as recrystallized pods and as fracture fillings. Bedding mostly regular but some microbands offset 2 mm or less by microfaults. Dip = 25 degrees.
568.76-569.1	Minor magnetite and silicate microbands in quartz-biotite schist. Minor streaks of garnet associated with epidote and pyrite are present. Bedding regular. Dip = 25 degrees.
569.1-569.2	Six mm silicate microband above alternating magnetite and schist microbands. Magnetite microbands 10 mm or less. Schist microbands 5 mm or less. Schist has a lower silicate content than the overlying silicate zone. Regularly bedded. Dip = 25 degrees.
569.2-569.27	Zone of strongly contorted magnetite microbands in schist. Modal analysis of thin section E625-0 from this interval showed it to consist of 50.8% quartz, 39.4% magnetite, 0.4% hematite, 7.8% biotite, 0.2% clinozoisite, and 1.4% calcite.
569.27-569.57	Quartz-biotite schist with minor silicate microbands.
569.57-572.72	Magnetite and silicate microbands interlayered with slightly to nonmagnetic quartz-biotite schist. Bedding mostly regular with strongly contorted zone from 570.48-571.35 m. Modal analysis of thin section E634-6 from a magnetite-rich zone in this interval

Depth in m	Description
	showed it to consist of 57% quartz, 32.2% magnetite, 1.6% hematite, 1% biotite, 0.2% clinozoisite, and 8% calcite.
572.2-573.1	Nonmagnetic quartz-biotite schist with minor magnetite and silicate microbands. Microbands are 2 mm or less.
573.1-579.2	Magnetite, specular hematite, and magnetite-specular hematite microbands interlayered with schist and minor silicate microbands. Oxide microbands 12 mm or less. Bedding ranges from regular to highly contorted. Dip = 20 degrees. Modal analysis of thin section E644-3 from this interval showed it to consist of 40.6% quartz, 34.8% magnetite, 1.4% specular hematite, and 23.2% calcite. Modal analysis of thin section E657-4 from this interval showed it to consist of 47.2% quartz, 45.2% magnetite, 2% chlorite, 2.6% clinozoisite, 0.2% grunerite, and 2.8% calcite.
579.2-589.18	Slightly to nonmagnetic quartz-biotite schist with minor magnetite and silicate microbands. Microbands 12 mm or less. Bedding mostly regular but some zones show strong distortions. Dip = 20 degrees. Modal analysis of thin section E673-0 from a magnetite-silicate zone in this interval showed it to consist of 55.2% quartz, 25.6% magnetite, 0.6% hematite, 7.2% biotite, 0.6% clinozoisite, 10% grunerite, and 0.8% oligoclase. Thin section E683-8 from another magnetite-silicate zone in this interval showed it to consist of 45.2% quartz, 35.2% magnetite, 1.4% hematite, 2.4% chlorite, 11.4% clinozoisite, 4% grunerite, 0.2% calcite, and 0.2% pyrite. Modal analysis of thin section E690-10 from a schist zone in this interval showed it to consist of 69% quartz, 4% magnetite, 15% biotite, 0.2% clinozoisite, 11% grunerite, 0.2% pyrite, and 0.6% oligoclase.

APPENDIX B

MODAL ANALYSES

A = THIN SECTION FROM AKRA CORE
E = THIN SECTION FROM HENSEL CORE

VOLUME PERCENT
Thin Section Number / Depth in m

Minerals	A8-2 426.2	A26-2 433.8	A35-3 438.8	A44-5 442.4	A87-2 454.5	A98-7 457.9
Quartz	50.0	44.0	85.8	43.0	49.0	64.4
Magnetite	1.0	1.0		32.8	1.0	3.0
Hematite	22.8	29.6				
Biotite			0.6	4.2	30.8	31.8
Chlorite	15.4	25.2		13.6		
Clinozoisite					19.2	
Grunerite						
Calcite	8.4	0.2	13.4	4.4		
Pyrite						0.2
Plagioclase						0.2
Muscovite						0.4
Stilpnomelane		1.0				

Minerals	A106-8 460.2	A108-1 460.6	A110-6 461.3	A112-5 461.9	A121-10 464.2	A130-0 466.9
Quartz	60.8	35.2	52.0	52.4	51.8	61.8
Magnetite	17.0	33.2	25.0	35.0	19.8	14.2
Hematite						
Biotite	18.4	15.0	19.2	11.0	12.6	20.4
Chlorite						
Clinozoisite	2.4	16.0	2.4	1.4	15.0	2.4
Grunerite					0.4	
Calcite					0.4	
Pyrite	1.4	0.6	0.4	0.2		0.2
Plagioclase			0.8			0.6
Muscovite			0.2			0.4

Minerals	A131-10 467.5	A132-2 467.4	A133-7 468.0	A134-5 468.3	A139-11 469.9	A151-2 472.8
Quartz	51.4	61.0	50.2	53.4	52.6	68.4
Magnetite	27.3	21.4	26.6	19.4	20.6	6.4
Hematite						
Biotite	2.2	10.0	5.6	3.8	8.4	16.6
Chlorite						
Clinozoisite	9.8	9.2	9.8	10.2	6.8	8.4
Grunerite	8.2		6.6	4.0	0.2	
Calcite	1.2	6.8	1.2	9.2	3.0	0.2
Pyrite						
Plagioclase						
Muscovite						

Minerals	A161-2 475.8	A172-5 479.3	A175-9 481.3	A182-2 482.6	A211-1 487.7	A233-0 497.4
Quartz	57.8	57.0	81.2	62.0	67.6	64.4
Magnetite	1.0	3.0	0.2	1.4	0.2	7.6
Hematite			1.4			0.4
Biotite	12.6	31.2	9.4	33.8	26.8	21.6
Chlorite	4.2		0.6	1.4		
Clinozoisite	24.2	8.2	0.8	1.2		5.2
Grunerite					4.4	0.6
Calcite		0.4	1.8	0.2	0.2	0.2
Pyrite			4.4		0.8	
Plagioclase	0.2	0.2				

Minerals	A250-6 503.7	A250-10 503.8	A275-1 514.2	E1-2 387.4	E5-9 389.5	E26-6 392.9
Quartz	65.6	57.0	52.0	42.4	59.6	44.8
Magnetite	7.6	3.0	5.2	16.2	10.6	19.8
Hematite			0.2			0.2
Biotite	18.6	25.8	13.8	2.4	5.6	
Chlorite			0.2	12.2	9.6	
Clinozoisite	4.8	13.2	10.8	23.4	14.6	22.4
Grunerite	3.2	0.8	17.8			
Calcite	0.2	0.2		1.8		10.2
Pyrite						
Plagioclase				1.6		
Muscovite						
Almandite						2.6

Minerals	E37-6 398.4	E70-5 408.1	E79-8 410.6	E111-1 420.3	E140-5 429.5	E149-11 431.9
Quartz	66.0	52.2	56.8	59.2	46.8	58.8
Magnetite	15.0		16.8		17.0	0.2
Hematite	0.8				5.4	
Biotite	5.8	15.4	12.4	16.0		32.4
Chlorite					5.2	
Clinozoisite	8.4	1.0	6.0	2.2	13.2	4.2
Grunerite		23.8	7.8	16.0	9.8	
Calcite	0.2					
Pyrite						
Plagioclase	0.2	7.4		6.6	1.8	4.4
Muscovite						
Almandite						

Minerals	E171-5 438.6	E187-8 443.5	E196-8 446.2	E254-2 461.2	E260-11 444.2	E265-3 465.7
Quartz	55.8	64.6	36.8	46.6	41.0	65.0
Magnetite	26.0	29.0	43.6	31.2	4.6	10.0
Hematite	11.4	2.6	0.2	0.2		0.2
Biotite		0.6	11.8	12.2	10.4	
Chlorite		0.2	0.8	5.6	10.2	
Clinozoisite	1.8	1.6	6.8	9.0	30.6	0.2
Grunerite	0.6					
Calcite	1.6	1.4			2.4	13.6
Pyrite				0.2		
Plagioclase					0.8	
Muscovite						
Almandite						11.0

Minerals	E286-7 471.5	E300-7 475.2	E318-7 480.4	E338-4 486.2	E354-3 490.7	E375-1 496.8
Quartz	43.6	60.4	55.2	56.2	65.6	39.2
Magnetite	15.8	13.2	32.8	24.2	31.4	18.0
Hematite		11.2	4.0	13.6	0.6	10.0
Biotite	0.2					2.6
Chlorite	14.8		4.8			23.2
Clinozoisite	24.8	0.4			3.2	4.2
Grunerite			0.4		0.2	
Calcite		14.4	1.6	2.4	2.2	
Pyrite						2.4
Plagioclase	0.8					0.4
Muscovite						
Almandite						
Sillimanite			1.2			

Minerals	387-2.5 500.8	E401-5 504.4	E422-10 510.8	E443-6 516.9	E457-4 520.6	E482-9 528.2
Quartz	51.6	64.2	48.2	76.4	37.8	53.6
Magnetite	4.4		24.8	0.2	33.8	30.8
Hematite						0.2
Biotite	12.6	33.8	1.8	2.8		12.2
Chlorite			12.4		18.4	1.2
Clinozoisite	2.6	0.8	10.8	6.4	9.2	0.6
Grunerite	27.2			8.2		
Calcite	0.4		2.0	4.4		1.4
Pyrite	0.4	0.8			0.6	
Plagioclase		0.2		0.2	0.2	
Muscovite		0.2				
Almandite	0.8					
Sillimanite				1.4		

Minerals	E497-2 532.5	E502-10 533.7	E533-0 542.5	E545-8 546.5	E550-8 547.7	E570-4 553.5
Quartz	52.8	49.2	51.1	54.0	61.6	46.2
Magnetite	42.4	40.6	28.0	40.0	18.6	22.6
Hematite	0.2	5.0	3.1	2.0		
Biotite	1.6	0.2	4.1	0.8	3.2	21.0
Chlorite	0.2	0.6			6.4	3.2
Clinozoisite	0.6	0.6			5.2	0.6
Grunerite	1.6	2.8		1.8		
Calcite	0.6	1.0	13.6	1.0	4.2	4.6
Pyrite						
Plagioclase					0.8	

Minerals	E588-5 558.1	E604-8 563.6	E625-0 569.7	E634-6 572.7	E644-3 575.2	E657-4 578.8
Quartz	39.2	54.8	50.8	57.0	40.6	47.2
Magnetite	28.6	28.8	39.4	32.2	34.8	45.2
Hematite	0.2	0.2	0.4	1.6	1.4	
Biotite	9.0	3.0	7.8	1.0		
Chlorite	0.2					2.0
Clinozoisite	8.8	4.6	0.2	0.2		2.6
Grunerite	1.6					0.2
Calcite	1.0	7.0	1.4	8.0	23.2	2.8
Pyrite						
Plagioclase	0.2					

Minerals	E673-0 583.4	E683-8 587.0	E690-10 589.2
Quartz	55.2	45.2	69.0
Magnetite	25.6	35.2	4.0
Hematite	0.6	1.4	
Biotite	7.2		15.0
Chlorite		2.4	
Clinozoisite	0.6	11.4	0.2
Grunerite	10.0	4.0	11.0
Calcite		0.2	
Pyrite		0.2	0.2
Plagioclase	0.8		0.6
Muscovite			

REFERENCES

REFERENCES

Anderson, S. B., North Dakota Geological Survey: Personal communication, April 1975.

Anhaeusser, C. R., Mason, R., Viljoen, M. J., Viljoen, R. P., 1969, A reappraisal of some aspects of Precambrian shield geology: Geol. Soc. America Bull., v. 80, p. 2175-2200.

Cloud, P., 1973, Paleoecological significances of the banded iron-formation: Econ. Geology, v. 68, p. 1135-1143.

French, B. M., 1968, Progressive contact metamorphism of the Biwabik iron-formation, Mesabi range, Minnesota: Minnesota Geol. Survey Bull. 45, 103 p.

French, B. M., 1973, Mineral assemblages in diagenetic and low-grade metamorphic iron-formation: Econ. Geology, v. 68, p. 1063-1074.

Garrels, R. M., and Christ, C. L., 1965, Solutions, minerals, and equilibria: New York, Harper and Row, 450 p.

Goldich, S. S., 1973, Ages of Precambrian banded iron-formations: Econ. Geology, v. 68, p. 1126-1134.

Goldich, S. S., Nier, A. O., Baadsgaard, H., Hoffman, J. F., and Krueger, H. W., 1961, The Precambrian geology and geochronology of Minnesota: Minnesota Geol. Survey Bull. 41, 193 p.

Goodwin, A. M., 1973, Archean iron-formations and tectonic basins of the Canadian Shield: Econ. Geology, v. 68, p. 915-933.

Grout, F. F., 1929, The Saganaga Granite of Minnesota-Ontario: Jour. Geology, v. 37, p. 562-591.

Gunderson, J. N., and Schwartz, G. M., 1962, The geology of the metamorphosed Biwabik iron-formation, Eastern Mesabi district, Minnesota: Minnesota Geol. Survey Bull. 43, 139 p.

Hutchison, C. S., 1974, Laboratory handbook of petrographic techniques: New York, Wiley and Sons, 527 p.

Hyndman, D. W., 1972, Petrology of igneous and metamorphic rocks: New York, McGraw-Hill, 533 p.

James, H. L., 1954, Sedimentary facies of iron formation: Econ. Geology, v. 49, p. 235-294.

James, H. L., 1955, Zones of regional metamorphism in the Precambrian of northern Michigan: Geol. Soc. America Bull., v. 66, p. 1455-1488.

James, H. L., 1966, Chemistry of the iron-rich sedimentary rocks: U.S. Geol. Survey Prof. Paper 440-W, 61 p.

James, H. L., and Sims, P. K., 1973, Precambrian iron-formations of the world - introduction: Econ. Geology, v. 68, p. 913-914.

Klein, C., 1973, Changes in mineral assemblages with metamorphism of some banded Precambrian iron-formations: Econ. Geology, v. 68, p. 1075-1088.

Klinger, F. L., 1956, Geology of the Soudan mine and vicinity, Guide Book series, Precambrian of northeastern Minnesota: Geol. Soc. America, Minneapolis Mtg., p. 120-134.

Kranck, S. H., 1961, A study of phase equilibria in a metamorphic iron formation: Jour. Petrology, v. 2, p. 137-184.

Lidiak, E. G., Buried Precambrian rocks of North Dakota: in preparation.

Moore, W. L., and Karner, F. R., 1969, Magnetic anomalies in Pembina County, North Dakota: North Dakota Geol. Survey Report of Investigation 49, 7 p.

Moorhouse, W. W., 1959, The study of rocks in thin section: New York, Harper and Row, 514 p.

Schwartz, G. M., 1956, Summary of the Precambrian geology of northeastern Minnesota: Geol. Soc. America, Minneapolis Mtg., p. 1-9.

Schwartz, G. M., and Prokopovitch, N., 1956, Map of mineral resources of Minnesota: Minnesota Geol. Survey.

Short, M. N., 1940, Microscopic determination of the ore minerals: Geol. Survey Bull. 914, 314 p.

Sims, P. K., 1970, Geologic map of Minnesota: Minnesota Geol. Survey Misc. Map Series Map M-14.

Turner, F. J., 1968, Metamorphic petrology; mineralogical and field aspects: New York, McGraw-Hill, 403 p.

Turner, F. J., and Verhoogen, J., 1951, Igneous and metamorphic petrology: New York, McGraw-Hill, 602 p.

Van Hise, C. R., and Clements, J. M., 1901, The Vermillion iron-bearing district: U.S. Geol. Survey, 21st Annual Rept., pt. 3, p. 401-409.

Woollard, G. P., 1964, Bouger gravity anomaly map of North America: American Geophysical Union.